Study of Carbide Banding in 51CrV4 Spring Steel

S. Schuurmans

Master Thesis

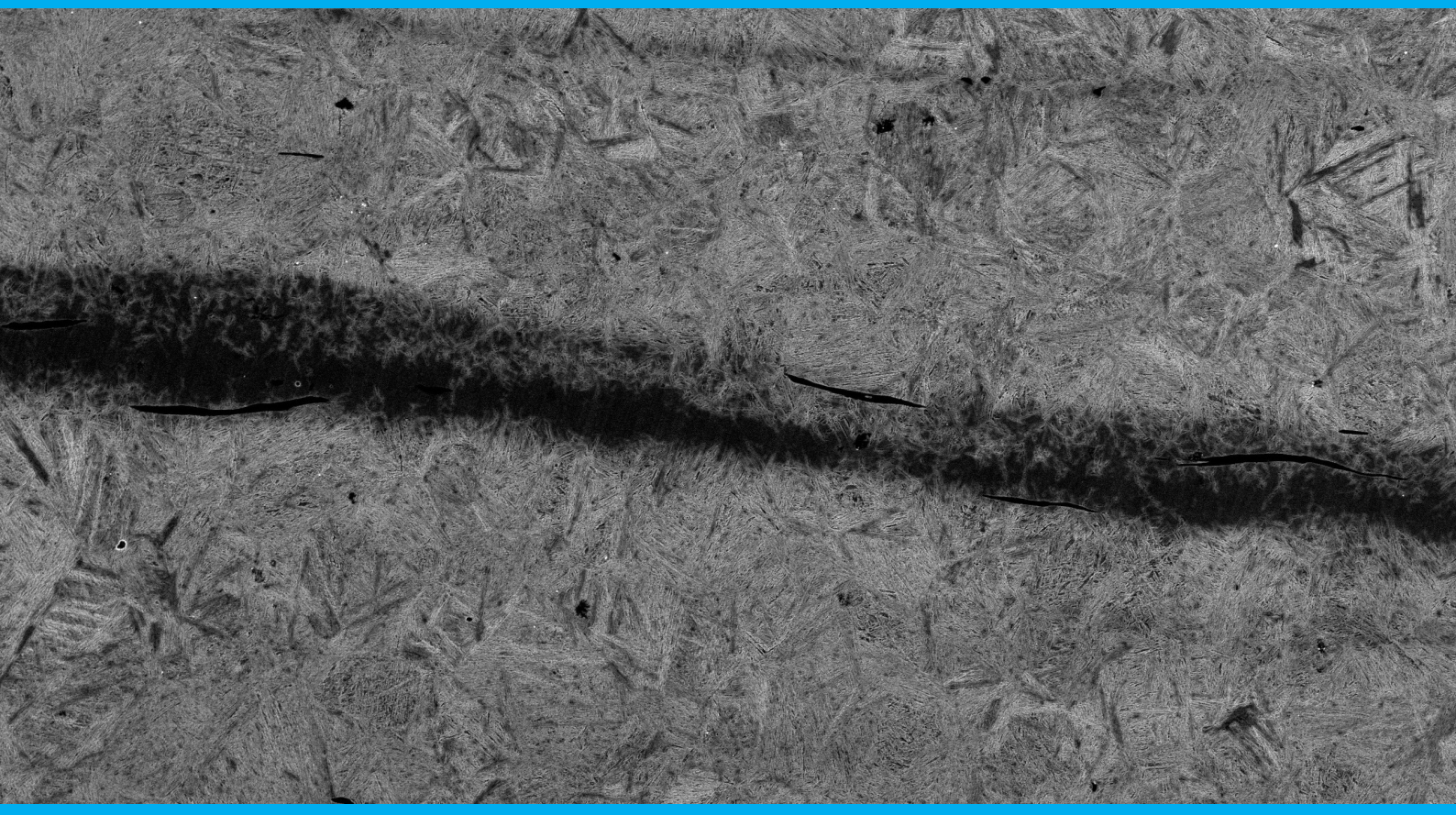

TU Delft

Study of Carbide Banding in 51CrV4 Spring Steel

by

S. Schuurmans

to obtain the degree of Master of Science

at the Delft University of Technology,

to be defended publicly on Monday August 29, 2022 at 9:30 AM.

Student number:	4364902	
Project duration:	December 1, 2021 – August 29, 2022	
Thesis committee:	Dr. ir. S.E. Offerman,	TU Delft, supervisor
	Dr. L. Zhao,	VDL Weweler, supervisor
	Prof. dr. ir. J. Sietsma,	TU Delft

An electronic version of this thesis is available at http://repository.tudelft.nl/.

TU Delft

Preface

I would like to thank Erik Offerman and Lie Zhao for their supervision during my master's thesis project. Their input, feedback and expertise were invaluable for a successful completion of my thesis.

I would like to thank Richard Huizenga for his help during XRD analysis and I would like to thank Kees Kwakernaak for his during EPMA measurements. I would also like to thank the many lab assistants of the material science lab for their help in giving me lab instructions and assistance during my research.

Finally, I would like to thank my family and friends who supported me with insight and inspiration during my research and throughout my studies.

S. Schuurmans
Delft, August 2022

Abstract

51CrV4 is a spring steel commonly used for the production of trailing arms in the suspension assembly of trucks. It is essential for these products to be predictable and reliable. The presence of carbide banding in 51CrV4 steel can be detrimental to this predictable and reliable behavior. Therefore, in this research, the formation of carbide-banded microstructure in 51CrV4 steel will be investigated. The bending stresses undergone by trailing arms make it crucial to understand the relationship between surface depth and carbide band formation. Therefore, the goal of this research is to understand the relation between the surface depth and band formation in 51CrV4 steel and how banding differs among 51CrV4 steel from different manufacturers. This was done using a variety of testing methods which include microscopy, hardness, XRD, SEM, EDS and EPMA. These testing methods were used to understand the formation of carbide bands in 51CrV4 as well as the underlying physical properties that lead to the carbide band formation. Overall, a significant difference could be seen in the formation of carbide bands across the steel from different manufacturers. These differences in carbide banding properties could be clearly linked to the difference in the physical properties of the steels. The depth at which carbide band formation tends to start could be most clearly related to the micro-segregation peak concentration. Furthermore, the manner in which the carbide bands are built up along the surface depth could be most clearly related to the chromium concentration in the carbide banded regions. Finally, it was found that chromium is expected to be the primary carbide former in this steel as the formation of carbide bands is closely and consistently related to an increased presence of chromium.

Contents

List of Figures

List of Tables

1

Introduction

VDL Weweler is a company that specializes in the manufacturing of automotive trailing arms. The trailing arms developed by VDL Weweler are often built with the use of 51CrV4 steel. Which is commonly used in the automotive industry as a spring steel. Recently, the presence of banded regions in many of the products developed using 51Crv4 steel has been discovered. The presence of this banding behavior can be detrimental to the product as it can lead to premature failure of the trailing arm. Therefore, it is crucial to research the degree of banding that occurs in these trailing arms.

Microstructural banding in steel is defined as a manifestation of alternating layers of different microstructures aligned parallel to the rolling direction [1]. The formation of this banded microstructure results in the mechanical properties of the steel having directional inhomogeneity which is referred to as anisotropy. Typically, it is therefore desirable to avoid steel banding. However, this is not always possible.

Steel banding has been present in steel since the early days of steelmaking before much was understood about the mechanics of steel. In many of these early steels, banding provided positive mechanical properties that early blacksmiths were able to exploit, due to its anisotropic behavior.

Steel banding is a microstructural phenomenon that has long been found in steels but has not been fully understood. In the 1960s and 1970s, much effort was put into understanding how banding originates in steels and to understand how it can be avoided. Nowadays steel banding is much better understood. Where steel banding originates from and how many parameters of the steel-making process affect the formation and size of steel bands are well understood. It is now understood that steel banding originates from the occurrence of segregation of alloying elements in steel. This is partially dependent on whether alloying elements are austenite stabilizers or ferrite stabilizers. In regions where austenite stabilizing elements (Ni, Co, Mn, Cu, C, and N) are in abundance, austenite and microstructures that will form at lower temperatures such as martensite, pearlite, and bainite are more likely to be present. Whilst in regions where ferrite stabilizing elements (Si, Cr, W, Mo, P, Al, Sn, Sb, Al, Zr, Nb, B, S, and Ce) are prevalent, ferrite is most likely to form [25]. The segregation of these alloying elements typically occurs during continuous cooling of slabs or other forms of large steel components. During this process, the steel solidifies from the surface inwards and sections of the microstructure solidify in a dendritic manner. The dendritic solidification results in the alloying elements segregating to the interdendritic regions as well as towards the center of the slab [28].

Micro-segregation is not the only prerequisite for banding to occur, however. The material still has to be processed further in order to elongate the material. This is most commonly done by the hot rolling of the material. The reason why this processing step is a prerequisite for banding to occur is that elongation of the grains in the rolling direction still has to occur. This elongation of the grains is what transforms

the microstructure into one with alternating bands of different phases [16].

For this research 51CrV4 steel will be the focus. 51CrV4 is classified as a quench and tempered steel type. It is primarily used in applications where components undergo high stresses and require excellent elongation [2]. Therefore, high strength and fracture toughness are prioritized. One such application is automotive spring steel. 51CrV4 is a medium carbon spring steel with substantial amounts of Silicon, Manganese, Phosphorous, Chromium, and Vanadium. Silicon, Manganese, and Chromium are of particular importance as segregation of these elements typically have the most significant impact on banding [14].

In this report, we will first discuss the background information and what is already known about microstructural banding and how that is related to 51CrV4 steel. From this, we will analyze the steel samples provided using several characterization techniques. These techniques include microscopy, hardness testing, EPMA, SEM, XRD and EDS. This will help us understand the banding characteristics in the steel samples and how it is impacted by the underlying microstructural properties.

The primary goal of the research is to understand the relation between the surface depth and band formation in 51CrV4 steel and how banding differs for 51CrV4 steel from different manufacturers. In order to achieve this, sub-research goals were set up, namely, to correlate the impact of surface depth to band formation, investigate the underlying micro-segregation and its impact on band formation, identify the predominate banding microstructure found in 51CrV4 steel and determine the depth at which band formation starts.

2

Background

2.1. Material Properties 51CrV4 Steel

Steel is found in many different compositions of alloys. These different alloying elements are present in steel for a variety of reasons such as to stabilize particular microstructures as well as improve specific mechanical properties and many more. The alloying elements found in the 51CrV4 steel, which will be the focus of this research, can be found in table 2.1. The addition of carbon is essential to what makes an iron alloy steel. What makes carbon so important is its impact on the strength, hardness, ductility, and other aspects of the mechanical properties of steel. Furthermore, carbon is essential to the microstructural development of steel as it is much more diffusive throughout the material than other alloying elements. Chromium and Manganese are the most significant alloying elements present as both typically have a weight % around 1%. There is also a smaller, yet still relevant, fraction of vanadium present in the material. Manganese is primarily added to improve the strength, hardenability, and machineability of steel. The addition of chromium as a steel alloy is primarily in order to improve the corrosion resistance of the steel. Chromium and Manganese are both strong austenite stabilizers mostly due to their affinity with carbon. The primary carbide formers in 51CrV4 steel are Chromium and Vanadium.

Table 2.1: Chemical composition of 51CrV4 steel

Alloying Elements:	C	Mn	Si	P	S	Cr	V
Max (wt.%)	0.55	1.1	0.40	0.025	0.025	1.2	0.25
Min (wt.%)	0.47	0.7	0	0	0	0.9	0.10

2.2. Band Formation and the Impact of Processing

Steel production goes through a rigorous process in order to achieve the selected shape and microstructure. Modern-day steels typically go through primary and secondary steelmaking steps in order to obtain the required amounts of alloying elements as well as improve the steel quality by removing any undesired remnants. These steps are critical for determining the contents of the alloying elements. As certain alloying elements are essential for banding to take place. The micro-segregation of these alloying elements does not occur until a later stage, namely, during the casting phase of steelmaking is where micro-segregation primarily occurs. The nature of how this micro-segregation occurs during casting will be discussed later in this section. Micro-segregation of alloying elements alone is not the only requirement for band formation to occur. Subsequent forming steps are also crucial to consider for band formation. For band formation to occur the hot-rolling process is necessary. This is because

the elongation of grains is required for a microstructure to be considered banded. Furthermore, post-processing treatments are also important to consider as these processes can play an important role in the type of banding which is present as well as banding severity.

2.2.1. Casting

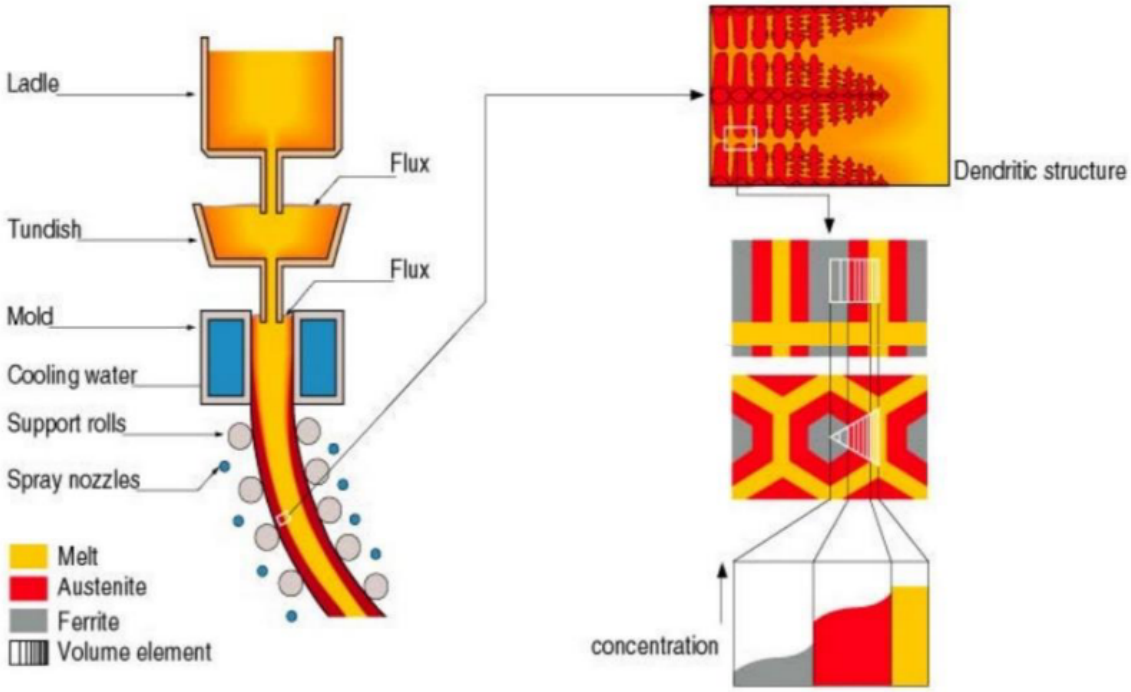

Figure 2.1: Schematic overview of solidification and segregation during a continuous casting process [13].

During casting processes, liquid steel is initially cooled and partially solidified in a water-cooled copper mold. Subsequently, the surface is rapidly cooled with a water spray increasing the shell thickness from the outside towards the center of the slab. This leads to a steep temperature gradient within the slab. A schematic overview of the solidification and segregation process during continuous casting can be seen in figure 2.1. The steep temperature gradient present results in differing grain formation mechanisms at different depths in the material. At the surface, high cooling rates are achieved leading to the formation of fine grains. These grains grow into the liquid phase as the solid/liquid interface shifts towards the center of the slab. Eventually, the solid/liquid inter-phase becomes unstable and dendrites begin to grow ahead of the solid/liquid inter-phase which leads to the formation of a columnar structure [11]. The dendritic growth leads to the segregation of elements across the slab thickness. It also leads to the concentration of solute elements, with a partition coefficient less than unity, ahead of the dendrites increasing as they are rejected. This results in inter-dendritic regions with high solute content. Towards the center of the slab, the thermal gradient is reduced which results in the reduction in the dendritic growth rate. In this region dendrite tips that grow ahead of the solid/liquid interface fracture and float in the liquid phase. The remains of the dendrite tips act as nucleation sites for further solidification in the slab. This results in the formation of an equiaxed structure in the center of the slab. The resulting cross-section of the slab can be seen in figure 2.2a. Three distinct regions can be seen in this figure, namely, the fine grains formed at the surface formed from the high cooling rate experienced in this region; The columnar structure formed due to the growth of dendrites ahead of the solid/liquid interphase; As well as the equiaxed grains formed in the center of the slab. [11]

An illustration of the dendritic growth into the liquid phase can be found in figure 2.2b. The dendritic growth consists of the formation of both primary and secondary dendrite arms. This dendrite formation is one of the driving forces of band formation as it results in the micro and macro-segregation of alloying

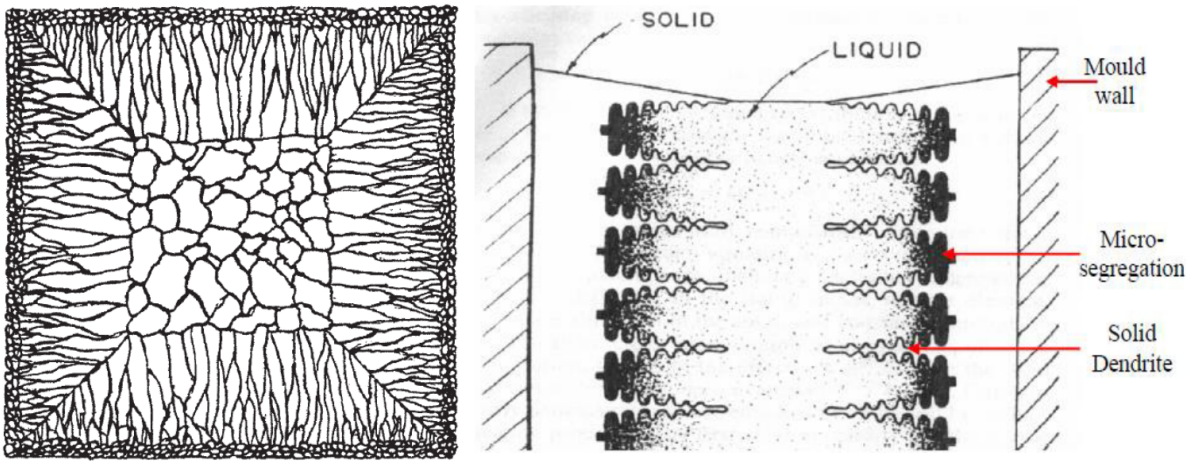

Figure 2.2: a) Schematic diagram of zones of crystal morphologies in an as solidified section of steel [11]. b) Sketch of Solidification in mold showing liquid, solid and dendrites [7].

elements in the steel.

2.2.2. Hot-rolling Process

The rolling process is important to discuss when considering the formation of bands. This process involves elongating the slab in the rolling direction whilst reducing the cross-sectional area. This is done by compressing the slab between two rotating rolls several times until the slab is in the desired shape. This process can be schematically visualized in figure 2.3

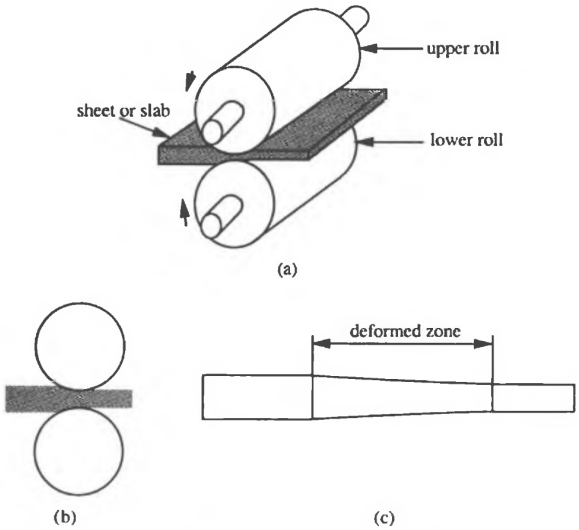

Figure 2.3: Schematic overview of the rolling process. [19]

This process can be done in two ways, hot-rolling or cold-rolling. Hot-rolling is done at an elevated above the austenite/ferrite transition temperature, typically above 900 °C. This is done to reduce work hardening during the deformation process as well as the residual stresses. Cold-rolling is done at room temperature and results in work hardening and residual stresses. These effects can be considered useful in some cases. For this research, primarily hot-rolling will be considered as it is more commonly used. Hot-rolling can be a strenuous process that requires many rolling cycles to achieve the desired shape as well as occasional re-heating processes in order to maintain the desired temperature range. During the rolling process, the slab is significantly deformed in the rolling direction. This results in the

elongation of grains along the deformed plane. This deformation of grains along the rolling direction has a significant impact on the mechanical properties of the materials in the rolling, transverse and longitudinal directions.

Hot-rolling having such a significant impact on the mechanical properties can make it difficult to understand the effects of band formation on the mechanical properties. As hot-rolling has been found to be one of the primary drivers of band formation, due to the elongation of grains in the rolling direction that occurs [1].

Hot rolling in the austenitic phase results in the formation of high and low solute content layers. These variations in solute content can lead to an inhomogeneous distribution of carbon in subsequent heat treatments. This effect is dependent on the content of the alloying elements. Certain elements, such as manganese, attract carbon whilst other elements, such as silicon, reject carbon. Carbon has a relatively high diffusion rate meaning thermodynamic equilibrium is typically achieved in the material. The other alloying elements have much lower diffusion rates such as the previously mentioned silicon and manganese. Therefore these elements are the primary cause of an inhomogeneous distribution of carbon throughout the microstructure. Furthermore, the increased presence of silicon will increase the transition temperature, A_3, whilst the presence of manganese will reduce the A_3 temperature. This has been found to be the cause of the formation of altering layers of ferrite and pearlite known as ferrite-pearlite banding. The relationship between microstructural banding and micro-chemical banding of manganese and silicon is clearly highlighted by Offerman et al. [14]. The results of their research can be seen in figure 2.4, in this figure the influence of micro-chemical segregation on the transformation temperatures and resulting band formation can be seen.

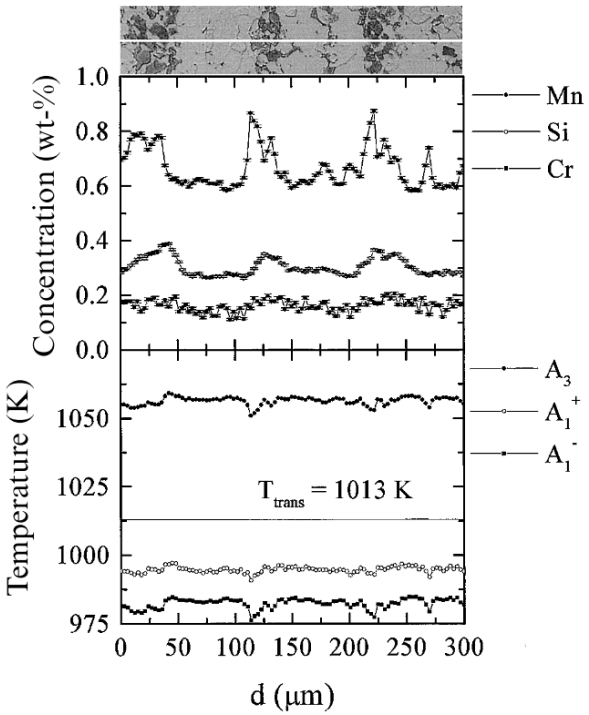

Figure 2.4: EPMA analysis of Mn, Si, and Cr and their effects on the local A_3, A_1^- and A_1^+ temperatures. [14]

Preßlinger researched the formation of bands during casting and hot-rolling of steel slabs. During his research, it was found that the primary dendrites grew parallel to the direction of heat flow. This results in the dendrites growing from the shell of the slab inwards during the casting process as shown in figure 2.2. As mentioned earlier, this results in the alloying elements being segregated to the inter-dendrite regions as well as towards the center of the slab. This is confirmed using by Preßlinger with the use of EPMA as seen in figure 2.5. In this figure, it can be seen that the minimum concentration of the alloying elements stays constant throughout the slab. However, the maximum concentration increases

with increased slab depth with a significant increase at the center of the slab.

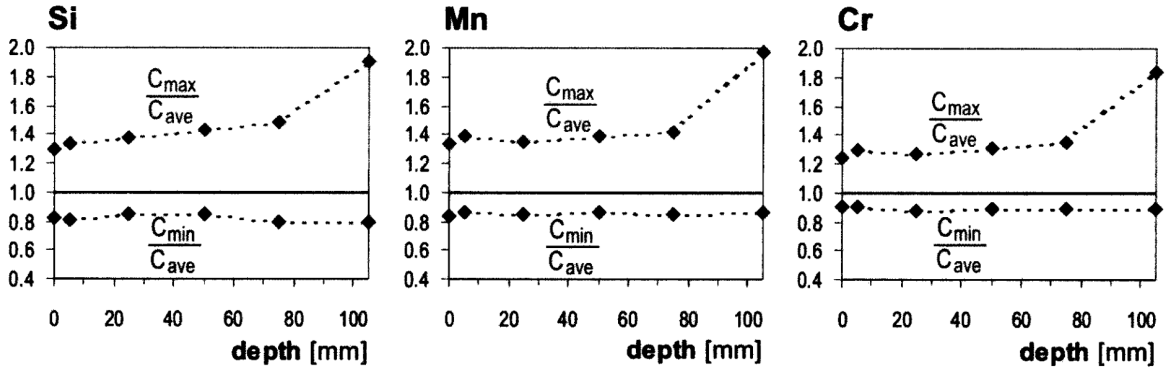

Figure 2.5: Segregation intensities as a function of the slab depth.[16]

Preßlinger also researched the development of the micro-chemical banding during the hot rolling process [16]. He did this using EPMA concentration mapping of the alloying elements present, namely, silicon, manganese, phosphorus, and chromium. In figure 2.6 The development of segregation of these different alloying elements can be seen.

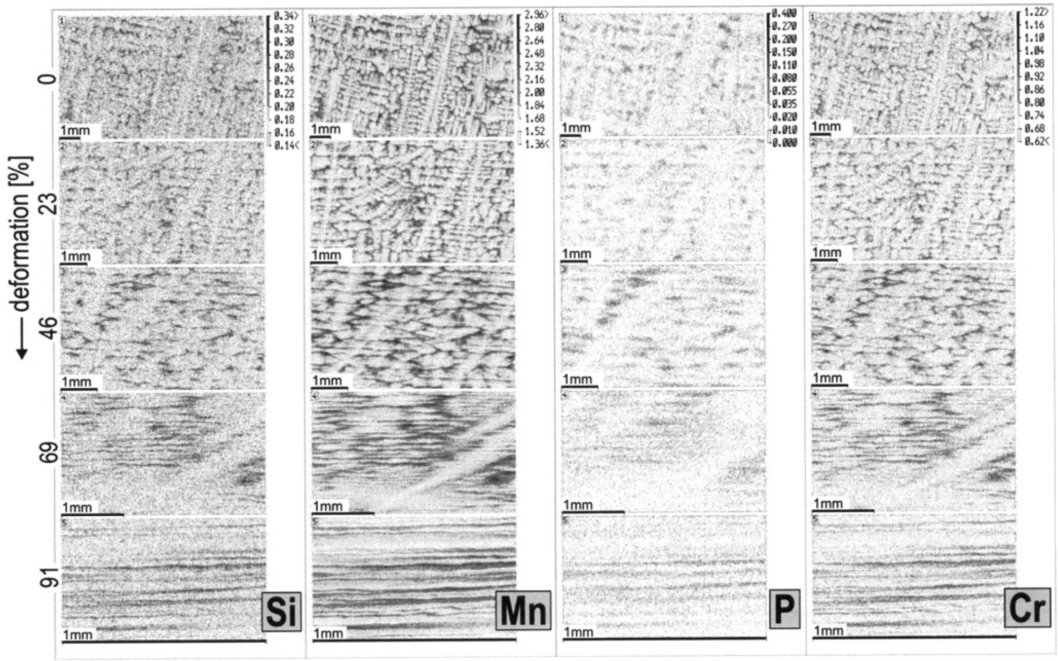

Figure 2.6: Overview of segregation for different alloying elements during hot-rolling.[16]

In the 0% deformation figures, the presence of regions with high and low fractions of alloying elements can be seen. These regions have a clear structure as a result of dendritic growth. Furthermore, the formation and elongation of bands can be seen with increasing deformation. Preßlinger concluded that banded microstructure was present at 70% elongation. He also researched the development of segregation during hot-rolling. As seen in figure 2.7 there was no significant change in the micro-segregation during hot-rolling.

2.2.3. Cooling Rate

The impact of the cooling rates has been briefly mentioned in previous sections but should be discussed further. The cooling rate plays an important role in the formation of banded microstructure. This is

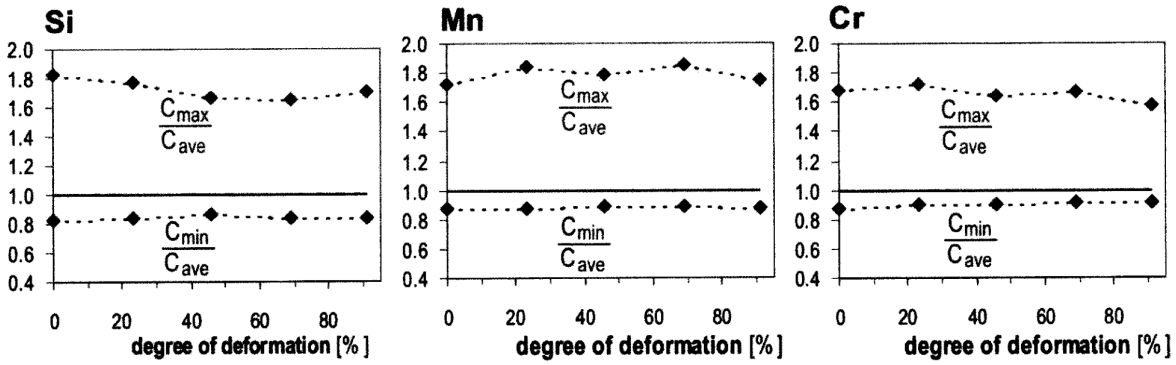

Figure 2.7: Segregation intensities as a function of the degree of deformation. [16]

primarily due to the importance of carbon diffusion in band formation. This is particularly the case for one of the most common types of band formation, namely ferrite-pearlite banding. This is because for clear band formation to occur carbon has to diffuse out of the ferrite phase in order for the pearlite microstructure to form. Carbide banding is another form of banding where the cooling rate can play a crucial role. As carbon diffusion is critical to the formation of carbides in steel.

One important factor to consider when looking at the effects of the cooling rate is that the cooling rates tend to be much lower towards the center of slabs. This means that whilst at the surface of a slab the cooling rate could be too high for banding to occur it can still form more towards the center of the slab. Finally, whilst the use of higher cooling rates is effective in limiting the diffusion of carbon during the initial heat treatments, micro-segregation still tends to be present and can still result in the formation of bands during subsequent heat treatments.

Turkdogan and Grange [26] found that the band width decreases with increasing cooling rate. Wu et al. researched the effects of cooling rate on carbide banding for high chromium content steels [29]. It was found that carbide banding decreases with an increasing cooling rate. Overall, they concluded that with increasing cooling rates the carbide band fraction was reduced and the carbide size in the banding region was also reduced.

Farhani et al. found that band formation can be suppressed even at lower cooling rates with cyclic partial phase transformation (CPPT) heat treatments [5]. It was concluded that controlled local enrichment of manganese occurs at the ferrite-pearlite interface due to the reverse transformation occurring as a result of the CPPT treatment.

Different heat treatments are also an effective way to achieve less conventional banding microstructures. One such example is the ferrite-martensite banded microstructure. This microstructure can be achieved when the material is held in the austenite-ferrite dual-phase region and is subsequently quenched. A similar heat treatment done by Tomita [24] found a ferrite-bainite microstructure. These treatments are however difficult to implement for larger components as the heat treatment would be inconsistent throughout the cross-section.

2.2.4. Grain Size

Grain size has been found to be of significance to the band formation in steels. Thompson and Howell [23] discussed the significance of the austenite grain size. Ferrite typically nucleates at the austenite grain boundary. Therefore, if the grain size is relatively small relative to the wavelength of micro-segregation, a sufficient nucleation site will be present. Because of this, ferrite will nucleate in regions where this is more favorable due to the alloying element's concentration or other factors. The ferrite grains will therefore continue to grow along the iso-concentration line, a region of similar alloying concentration until they impinge. This is followed by growth in the perpendicular direction. The remain-

ing austenite microstructure transforms into pearlite. This process is illustrated in figure 2.8. When the austenite grains are significantly larger than the micro-segregation wavelength, then the possible nucleation sites are limited and banding does not occur.

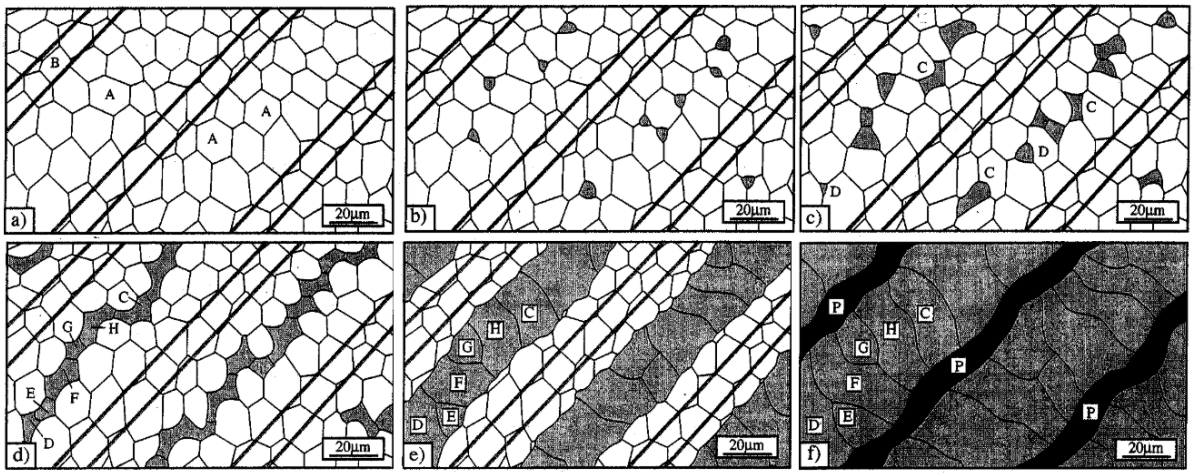

Figure 2.8: Illustration of the growth of ferrite grains during band formation. a) Fully austenite grain structure. b) Nucleation of ferrite grains in manganese lean regions. c) Growth of ferrite grains along the austenite grain boundary. d) Formation of ferrite 'slabs' in manganese lean regions. e) Completion of ferrite slab formation. f) Final microstructure with pearlite band formation in the former austenite region. [23]

2.2.5. Impact of Micro-segregation on Band Formation

The dependence of microstructural band formation on chemical segregation has been made clear, however, the origin of the segregation has been found to originate from different mechanisms. Early research into the formation of banded microstructures by Kirkaldy et al. found that there are two mechanisms for micro-chemical segregation, namely, pre-segregation and trans-segregation [9].

The theory of pre-segregation focuses on the uneven distribution of carbon before phase transformation occurs. This mechanism relies on the segregation of alloying elements which affect the activity of carbon. Due to the high diffusion rates of carbon in steel, the segregation of these alloying elements is the primary factor that determines the segregation of carbon. In regions with low carbon concentration ferrite is more likely to form [8].

The theory of trans-segregation focuses on the presence of alloying elements which impact the local transition temperature. The theory of trans-segregation assumes no pre-segregation takes place as it would otherwise be the dominant mechanism. Trans-segregation, therefore, assumes a consistent carbon concentration throughout the microstructure. The differences in local microstructure are determined by the presence of ferrite and austenite stabilizing elements. Ferrite stabilizing elements include phosphorus and silicon whilst manganese, nickel and chromium are austenite stabilizing elements. These elements are either ferrite or austenite stabilizing depending on their effects on the local transition temperature. Phosphorus and silicon have been found to increase the local transition temperature whilst manganese and chromium have been found to reduce the local transition temperature.

Further research has also found a third mechanism for band formation. This mechanism applies to steels with significant sulfur content. When both manganese and sulfur are present in steel MnS inclusions may form in the regions with high concentrations of manganese. The presence of these MnS inclusions attracts nearby manganese and therefore creates low-manganese areas around the inclusions. Because of this ferrite forms primarily in the areas surrounding the MnS inclusions.

2.2.6. Micro-segregation

Microstructural banding in steels is primarily a result of micro-segregation. Micro-segregation is a result of the composition of the phase during nucleation differing from the overall composition of the material. As the grain grows, the composition at the solid/liquid interface begins to shift towards the composition of the liquid phase due to the increasing alloying composition in the liquid phase and the subsequent shift in equilibrium as well as the lower temperatures present. This results in a gradient in the material composition throughout the grain which has been found to often occur in a dendritic manner. This process combined with subsequent hot rolling and heat treatment leads to banded microstructures in varying levels [27]. The micro-segregation in steels is dendritic in its nature. However, in deformed steels the formed bands are in line with the deformation plane and their alignment in the transverse and longitudinal directions are identical. The dendritic nature of the grains results in the grain branching outwards in a tree-branch-like manner. As the solid phase grows, carbon and other alloying elements are typically rejected and become concentrated in the inter-dendritic regions. The dendritic growth of the microstructure can be visualized in figure 2.9.

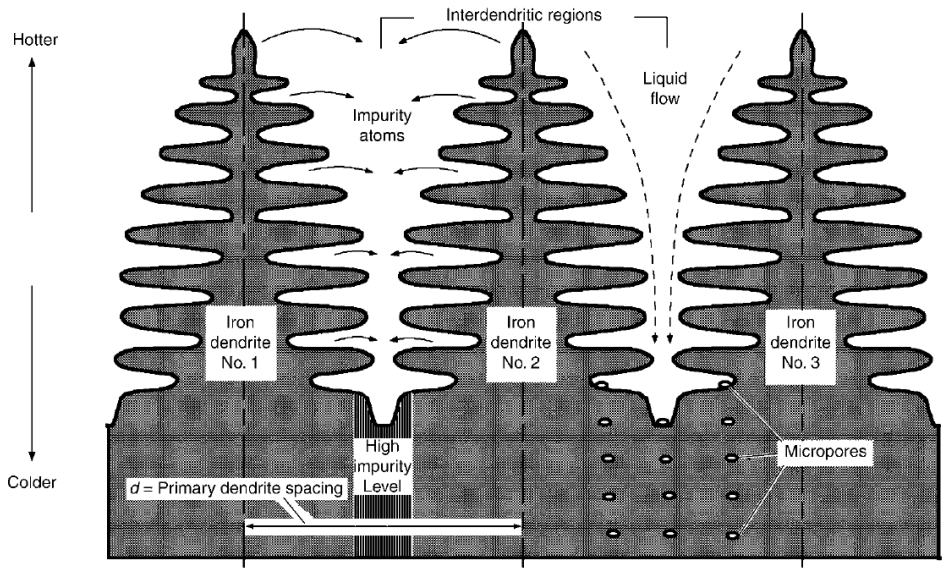

Figure 2.9: Schematic overview of dendritic grain growth [28]

Currently, research on micro-segregation has been focused on pearlite/ferrite (f/p) banded microstructures. This is due to the banded microstructure being present after a single cooling cycle when slower cooling rates are applied. However, studies have found that with subsequent heat cycles the banded structures also appear in steels that are initially quenched.

There is still debate about which aspect of dendritic growth has the greatest effect on micro-segregation. Verhoeven argues that the distance between the primary dendritic arms is the most important factor when determining the band size [27]. However, Krauss argues that secondary dendritic arm spacing is the most important factor for micro-segregation. The primary and secondary dendrite arm spacing can be schematically visualized in figure 2.10. Both of these factors are to a differing extent dependent on the cooling rate [12]. These parameters will be discussed in more detail in section 2.2.9.

2.2.7. Band Orientation

It is important to understand the orientation of band formation in order to analyze it and fully characterize its effects. As previously mentioned band formation tends to form along the rolling (RD) and transverse direction (TD), this behavior can be clearly seen in figure 2.11 (RD is indicated as LD in the figure). Furthermore the banded areas a typically very thin along the normal direction (ND). This difference in

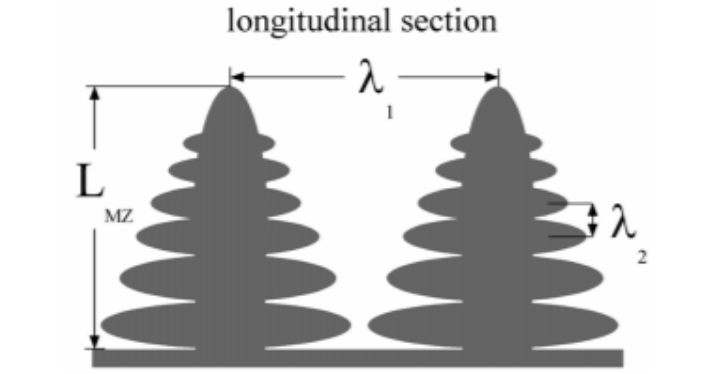

Figure 1. Definition of primary (λ_1) and secondary (λ_2) dendrite arm spacing.

Figure 2.10: Schematic overview of primary (λ_1) and secondary (λ_2) arm spacing. [21]

band shape along different directions is the basis of the anisotropic behavior which can make band formation so detrimental.

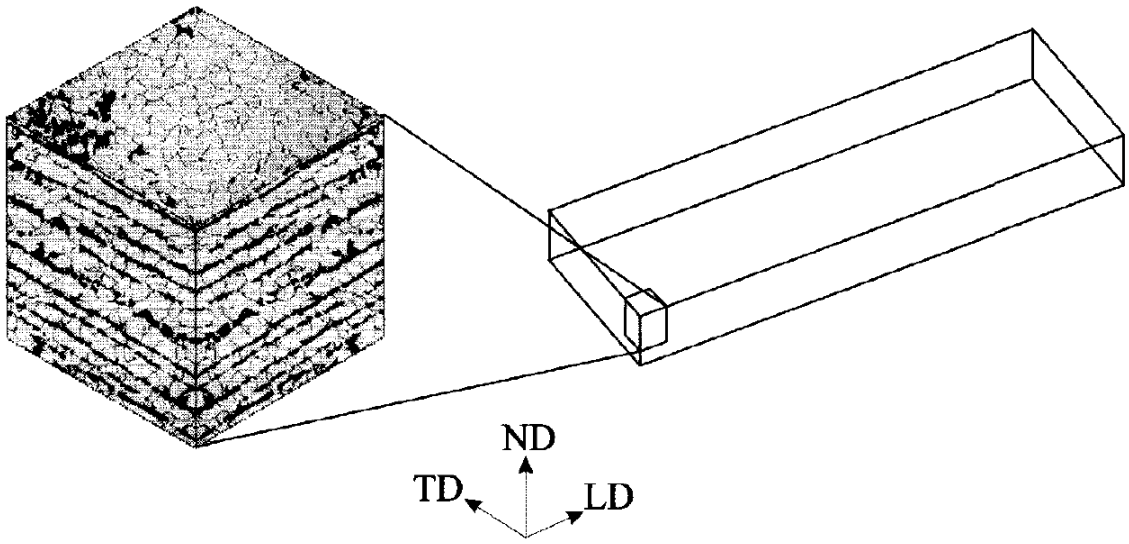

Figure 2.11: Schematic overview of how band formation typically occurs. Indicated in this figure are the transverse (TD), normal (ND) and longitudinal (LD) directions. The longitudinal direction is also often referred to as the rolling direction. [10]

2.2.8. Modeling Micro-segregation

The cooling rates experienced in steels where banding occurs are typically too high for complete solid-state solidification to take place. Because of this, the lever rule does not hold up and alternate models must be considered [8].

Over the years many models have been developed to help predict micro-segregation. Scheil developed an early model to help predict the behavior of micro-segregation during casting. However, this model neglected the presence of solid-state diffusion and reduced the model to one dimension by assuming a plate-like structure for the grains. Furthermore, this model makes certain assumptions like infinite diffusion in liquid, no undercooling, and a constant equilibrium partition coefficient. The equilibrium partition coefficient being constant results from the solidus and liquidus lines being assumed to be

constant as seen by equation 2.1. The Sheil equation helps determine the equilibrium concentration at the solid/liquid phase boundary as shown in equation 2.2 [20].

$$k = \frac{C_S}{C_L} \tag{2.1}$$

$$C_s^* = kC_0(1 - f_s)^{k-1} \tag{2.2}$$

In this equation c_s^* is the equilibrium alloy concentration at the phase boundary, C_0 is the average concentration of the alloy, k is the equilibrium partition coefficient, and f_s is the solid fraction. The equilibrium partition coefficient can be determined using equation 2.1. Scheil's model simplifies the problem to one dimension and the volume element growth is considered perpendicular to the growth direction as seen in figure 2.12. Scheil's equation is a simplified model and therefore does not provide an accurate image of the degree of micro-segregation. However, it can provide an upper limit of segregation profiles. Therefore, the Scheil model along with the lever rule provides an approximation of the possible segregation profiles. An example of these profiles can be seen in figure 2.13 b.

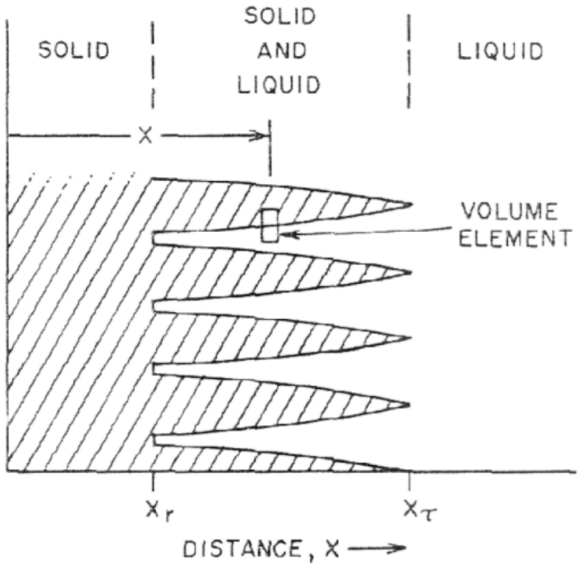

Figure 2.12: Schematic representation of the growing dendrites in the models considered. [3]

Brody and Flemming took Scheil's model further by accounting for solid-state diffusion. Their model uses the same geometry and many of the same approximations as Scheil's model. Diffusion is determined using Fick's second law. Furthermore, two interface velocity dependencies are assumed, namely, constant velocity and parabolic growth. This model assumes that solid-state diffusion does not affect the interface concentration gradient. Therefore, the interface concentration as a function of the fraction solid can be determined. In this model the ratio of the solid-state diffusion coefficient is defined as in equation 2.3 [3].

$$\omega = \frac{Dt_f}{L^2} \tag{2.3}$$

In this equation, D is the diffusion coefficient, t_f is the local settling time, and L is half of the dendritic arm spacing. The local settling time is considered the time between the onset of solidification until all of the material is solid. It is therefore inversely proportional to the cooling rate. Brody and Flemming's model assumes a constant solidification velocity. This results in the Brody and Flemming equation as found in equation 2.4 [3].

$$C_s^* = kC_0(1 - \frac{f_s}{1+\omega k})^{k-1} \tag{2.4}$$

In this equation, the micro-segregation is primarily dependent on the ratio of t_f and L^2. Whilst this model made further progress on Scheil's model there are still factors that haven't been factored in yet. One major flaw of the Brody and Flemming model is that it is unable to determine the influence of the cooling rate on the dendrite spacing.

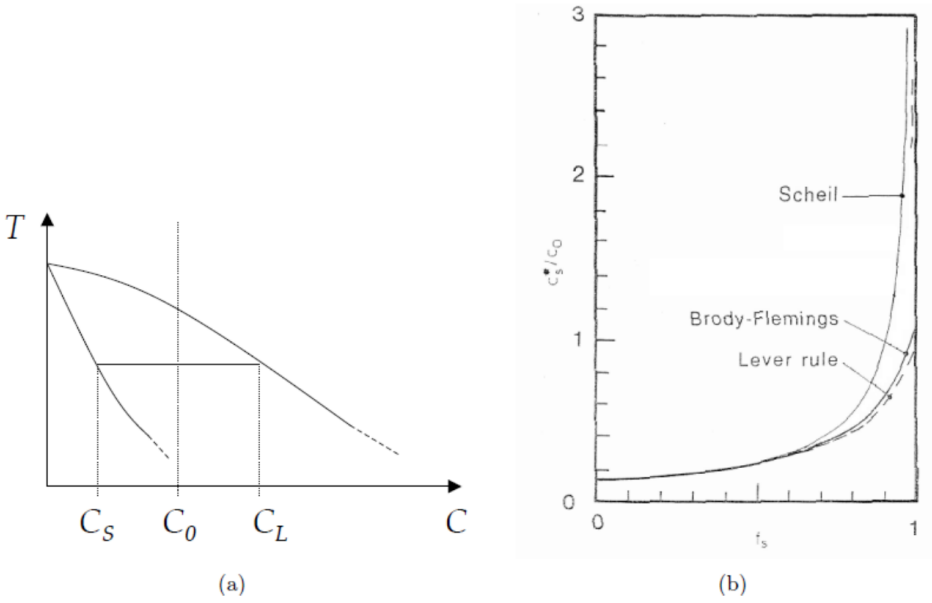

Figure 2.13: a) partial phase diagram showing the difference between solidus and liquidus lines. b) Overview of the solid to average concentration ratio, C_s/C_0 the solid fraction, F_S for the different models. [18]

In figure 2.13 an example of how the solidus and liquidus coefficients are determined is shown. In figure 2.13b a comparison of how the different models compare during the solidification process. The Scheil model and the lever rule typically determine the range of possibilities.

Many new models have since been proposed to make improvements on the limitations of these models [8]. The updated models were able to make further improvements in regards to the: dendrite geometry, solidification with moving phase boundaries, finite diffusion, the difference in density among interphases, undercooling at the dendrite tip, non-constant partition coefficient, and account for varying cooling conditions.

2.2.9. Dendrite Arm Spacing

As mentioned in the previous section one of the most important factors not considered by the early models is the dendrite arm spacing. The dendrites form as a result of constitutional undercooling and destabilization of the solid-liquid interface. The dendrite arm spacing is considered one of the most important factors which determine the degree of micro-segregation which in turn is critical to determining the amount of banding. The exact link between the amount of banding and dendrite arm spacing is still limited. Verhoeven [27] found that there is a relationship between the band width and the primary dendrite arm spacing. However, it was argued by Krauss [11] that the secondary arm spacing is the most important factor when determining the degree of inter-dendritic segregation. Primary and secondary dendrite spacing are both to different extents dependent on the cooling rate. It was shown by Jagle [8] that the secondary dendrite arm spacing is exponentially related to the local solidification by equation 2.5 [1].

$$\lambda_2 = Kt_f^h \tag{2.5}$$

In this equation λ_2 is the secondary dendrite arm spacing, t_f is the local solidification time, K is an empirical parameter and h has a value ranging from 0.3 to 0.6.

The dendrite arm spacing is dependent on many factors which make modeling and predicting it more complicated. Dendrite arm spacing is highly dependent on the cooling rate as seen in figure 2.14. As mentioned in section 2.2 the cooling rate can be drastically different depending on the surface depth. Because of this, the secondary dendrite arm spacing becomes much larger as seen in figure 2.15.

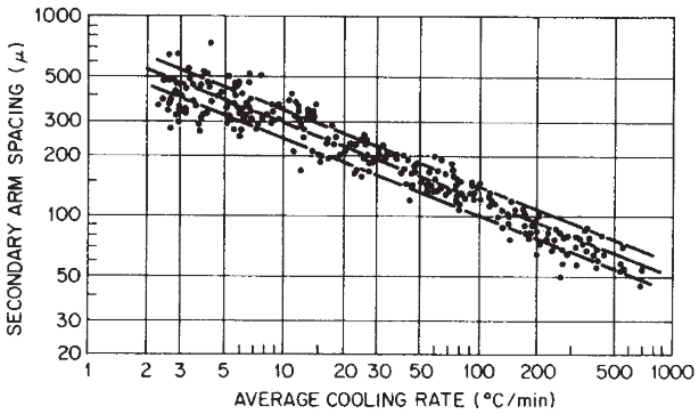

Figure 2.14: Secondary dendrite arm spacing as a function of cooling rate for commercial steels containing 0.1-0.9 wt.% C. [22]

Kattamis et al. found that the final dendrite spacing is primarily dependent on the coarsening kinetics. The reduction in the solid-liquid interphase area is the driving force behind coarsening. During this process, smaller dendrite arms remelt and the larger dendrite arms grow further. Simple models were developed in which the driving force for coarsening is inversely proportional to the dendrite arm spacing. This resulted in different models to account for coarsening, Feurer and Wunderlin developed equations 2.6 and 2.7 [6]. In these equations, t is the time and p_i are empirical parameters.

$$\lambda(t) = p_1 T^{1/3} \tag{2.6}$$

$$\lambda(t) = p_2 ln(1 + p_3 t) \tag{2.7}$$

Pierer and Bernhard experimentally investigated the effect of carbon on the secondary dendrite arm spacing. They conducted these experiments using steel with 0.28 wt.% Si, 1.32 wt.% Mn, 0.007 wt.% P and 0.007 wt.% S. For steels with a carbon range between 0.08 and 0.7 wt.% C, the empirical relation between the secondary dendrite arm spacing, carbon content and the solidification time can be seen in equation 2.8. This relationship can also be seen further in figure 2.16 [15].

$$\lambda_2(\mu m) = (23.7 - 13.1 * (wt.\%C)^{\frac{1}{3}}) t_f^{\frac{1}{3}} \tag{2.8}$$

Preßlinger researched the relationship with surface depth of secondary dendrite arm spacing. His measurements also accounted for the manganese concentration at varying surface depths. His experiments resulted in the relationship found in figure 2.17 [17]. His results show a clear increase in secondary dendrite arm spacing further away from the surface of steel slabs. This can be best explained by differing cooling rates experienced throughout the slab as a result of thermal gradients experienced.

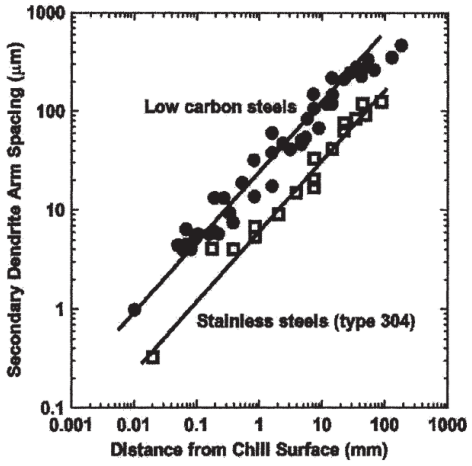

Figure 2.15: Secondary dendrite arm spacing as a function of distance from the surface of steel for various low-carbon and stainless steels. [4]

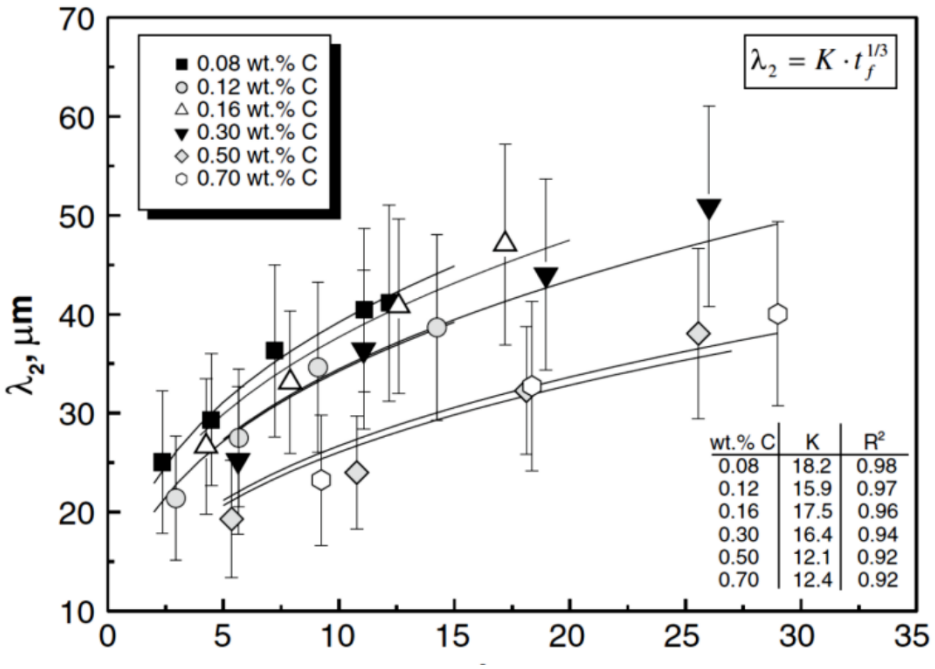

Figure 2.16: The relationship between secondary dendrite arm spacing and local solidification times for steels with different carbon content. [15]

2.2.10. Nucleation and Growth Model

Offerman et al. used their research into the micro-segregation of micro-chemical banding and its influence on local transition temperature and band formation to derive a nucleation and growth model for band formation. They derived nucleation and growth criteria for the formation of microstructural bands using the classical nucleation theory for the rate of ferrite nucleation seen in equation 2.9.

$$\frac{dN}{dt} = N_n \frac{kT}{h} exp(-\frac{\Delta G^* \mu}{k_b T}) exp(\frac{Q_d}{k_b T}) \tag{2.9}$$

In equation 2.9, N is the number of nuclei, N_n is the number of potential nucleation sites, k_b is the

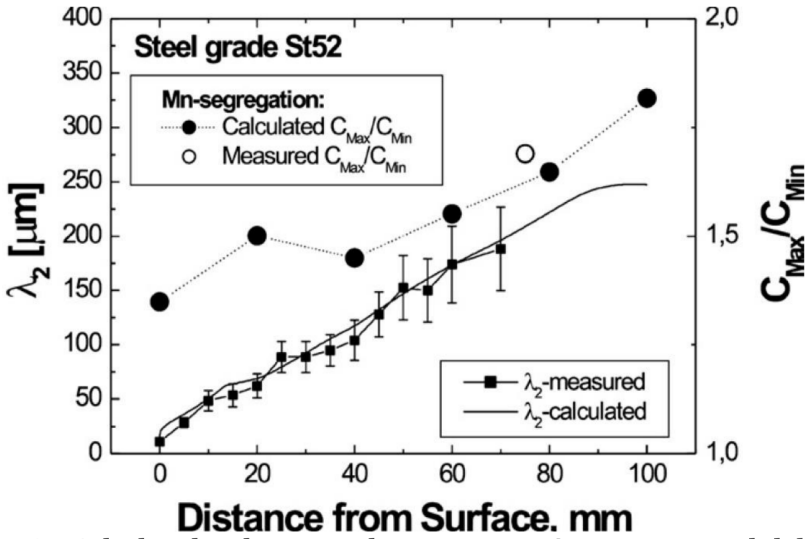

Figure 2.17: Calculated and measured Mn concentration across a steel slab. [17]

Boltzmann constant, h is Planck's constant, $\mu = 10^{-4}$ is a scaling factor and Q_D is the activation energy for self-diffusion. This parameter is important to consider as the formation of microstructural bands is dependent on sufficient nucleation sites being present. Offerman et al. consider ΔG^* by approximating the austenite grains as tetrakaidecahedrons, resulting in the energy barrier, ΔG^*, found in figure 2.10.

$$\Delta G^* = \frac{4(z_2\gamma_{\alpha\gamma} - Z_2\gamma_{\gamma\gamma})^3}{27Z_3\Delta G_V^2} \tag{2.10}$$

In this equation, $\gamma_{\alpha\gamma} = 0.6JM^{-2}$ is the surface free energy of the austenite/ferrite interface, $\gamma_{\gamma\gamma} = 0.85JM^{-2}$ is the surface energy of an austenite grain boundary and z_1, z_2, and z_3 are geometrical parameters that are dependent on the nucleation site for the austenite grain (boundary, edge, or corner). For a tetrakaidecahedron this can be approximated to $z_1 = 0.72, z_2 = 1.3$ and $z_3 = 0.096$. ΔG_V was approximated using Scientific Group Thermodata Europe (SGTE).

$$r = \frac{(\frac{dN}{dt})_{A_{3max}} - (\frac{dN}{dt})_{A_{3min}}}{(dN/dt)_{A_{3max}}} = 1 - exp[\frac{\mu}{kT}(\Delta G^*_{A_{3max}} - G^*_{A_{3min}})] \tag{2.11}$$

Equation 2.11 can be used to determine the relative difference, r, between ferrite nucleation where the, A_3, transition temperature, is maximum and minimum. Offerman et al. then compared r for two EPMA results and concluded that as seen in figure 2.18 that the critical undercooling for band formation to occur is between 953 K and 961 K for the samples analyzed.

In their model Offerman et al. also considered the importance of carbon diffusion in austenite as even if the relative difference in ferrite nucleation between regions is great enough for band formation, bands may still not completely form if carbon can not diffuse over the necessary distance. Therefore they used equation 2.12 to estimate the distance at which carbon can diffuse in the austenite phase.

$$d \approx (D_C^\gamma t)^{1/2} \tag{2.12}$$

In equation 2.12, d is the distance carbon can diffuse, D_C^γ is the carbon diffusion coefficient in austenite and t is the time elapsed before pearlite formation starts. Offerman et al. used equation 2.13 to

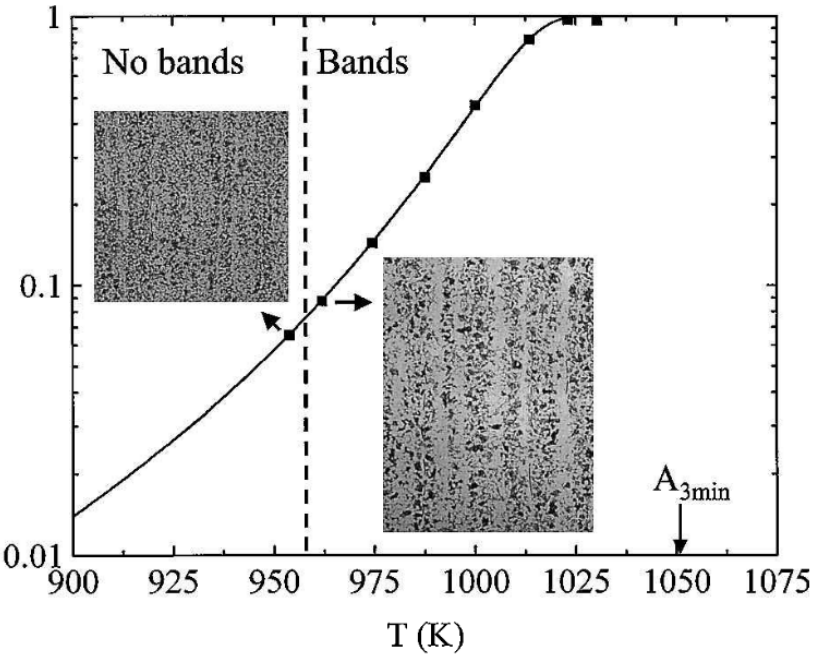

Figure 2.18: Relative difference of ferrite nucleation rate, r, as a function of isothermal transformation temperature, T. The dotted line represents the critical undercooling for band formation to occur. [14]

estimate the diffusion coefficient of carbon in austenite nominal carbon concentration and temperature they considered. Where they used equation 2.14 to estimate site fraction of carbon in the interstitial sublattice, Y_C (X_C = 0.016704).

$$D_C^{\gamma}(m^2/s) = 4.53 * 10^{-7}(1 + y_c(1 - y_c) * 8339.9 * T^{-1}) * exp[-(T^{-1} - 2.221 * 10^{-4})(17767 - 26436 * Y_C)] \quad (2.13)$$

$$Y_C = X_C/(1 - X_C) \quad (2.14)$$

Finally, they considered that the width of regions with high A_3 temperatures which are required for band formation can be estimated by the parameter w, which refers to the wavelength of chemical bands. Therefore the maximum distance carbon is required to diffuse can be estimated by equation 2.15.

$$d_C = w/2 \quad (2.15)$$

3

Experimental

3.1. Sample

In order to ensure that the results found during this research are accurate and reliable, it is essential to extract and process the samples in a way that limits the effect of any external variables. The steps are taken to ensure this, will be explained further in this section.

3.1.1. Processing

The trailing arms for this investigation were supplied by VDL Weweler. The processing steps undergone for the different trailing arms differed somewhat. However, all trailing arms used had been processed up to the final heat treatment stage, after which the further processing steps (shot-peening, painting, etc.) are not relevant for this research. Furthermore, these processing steps would only have an impact on the surface of the microstructure. There are also slight variations in the processing steps which are more relevant for the microstructure of the steel (hot-rolling, heating temperatures, etc.). However, trailing arms were used where this was as similar as possible and samples were extracted to diminish the effects of these differences.

Table 3.1: Chemical composition of 51CrV4 steel from different manufacturers (wt.%).

	C	Si	Mn	P	S	Cr	Mo	Ni	Al	Cu	Sn	V
SL:	0.51	0.26	1.07	0.012	0.008	1.15	0.03	0.13	0.002	0.15	0.008	0.110
SC:	0.51	0.31	1.02	0.017	0.002	1.13	-	0.19	0.008	0.24	0.014	0.131
SK:	0.54	0.30	0.98	0.011	0.012	1.15	0.03	0.10	0.007	0.19	0.012	0.110
KG:	0.52	0.34	0.99	0.007	0.001	1.13	0.003	0.08	0.016	0.09	0.011	0.137

3.1.2. Sample Preparation

Sample Extraction

Sample extraction was done from individual trailing arms provided by VDL Weweler. The samples were extracted from trailing arms similar to the one seen in figure 3.1b. These trailing arms are part of the suspension assembly for trucks, which VDL Weweler specializes in building. The suspension assembly system can be seen in figure 3.1a. These trailing arms were each constructed with steel from different steel manufacturers. These steels undergo further manufacturing by VDL Weweler. This manufacturing

(a) VDL Suspension Assembly

(b) VDL Trailing Arm

Figure 3.1: Schematic overview of the a) Suspension assembly and b) Trailing arm found in the suspension assembly.

process is slightly different for the individual trailing arms in terms of the heat treatments, hot rolling processes and further steps undergone. Therefore, the samples used for this research needed to be as similar as possible. This resulted in the samples being extracted from the region of the trailing arm where the thickness was greatest. This was done to maximize the area where samples could be extracted whilst having a similar thickness. Furthermore, this helps to determine the effects of the different steel suppliers on the final microstructure of the trailing arm as the manufacturing process done by VDL is not as significant due to the steel not being heated beyond the melting temperature, which would be necessary to achieve significant alloying element diffusion. Sample extraction was done to view the transverse face of the microstructure. The transverse surface was selected as the microstructural bands tend to be elongated in the rolling direction. Furthermore, the normal direction is important to view as it should provide the clearest indication of how the microstructural bands develop at different surface depths. A schematic overview of how the samples were extracted from the overview, as well as their orientation, can be found in figure 3.2. The different steel manufactured is referenced as KG, SC, SK and SL. For each steel manufacturer, three samples were extracted, referenced as A, B and C. These samples were further subdivided into upper (U), middle (M) and lower (L) sections.

In order to analyze the microstructural bands present in the 51CrV4 steel, many steps are required to prepare the sample for microscopy analysis, mechanical analysis and EPMA. The samples were cut from suspension arms and therefore have fully gone through the production process prior to analysis. Samples were cut from the suspension arm by making two large cuts along the normal direction in the regions where the lowest amount of additional deformation has occurred during processing by VDL as seen in figure 3.2a. Subsequently, the main samples are removed, previously referred to as samples A, B and C. This is done make four cuts along the normal direction as seen in figure 3.2b and 3.2c. The material is then cut further along the rolling direction to create sub-samples U, M and L as seen in figure 3.2d.

Table 3.2: Overview of the sample thickness of the different samples used. The difference is a function of the varying thicknesses of the trailing arms.

	KG	SC	SK	SL
Sample thickness (mm)	44.0	48.3	48.2	54.1

The samples used were extracted from trailing arms provided by VDL Weweler. The trailing arms used were selected as the heat treatment and manufacturing process were as similar as possible across the samples. The dimensions of the trailing arms tended to differ somewhat, however. The samples were extracted from regions that were as similar as possible. However, the sample dimensions did still differ somewhat for the different manufacturers. The most important difference between these samples which must be accounted for is the sample thickness. This is the smallest dimension for the trailing arms and therefore is most critical to the difference in cooling rates at the surface compared to the center. This would subsequently have an impact on the microstructures which form at the center of the samples. The thicknesses of the samples used can be seen in table 3.2. The KG samples are slightly smaller compared to the other samples while the SL samples are slightly larger. The impact this has on the microstructure and mechanical properties of the samples will be considered when discussing

(a) Sample extraction form trailing arm.

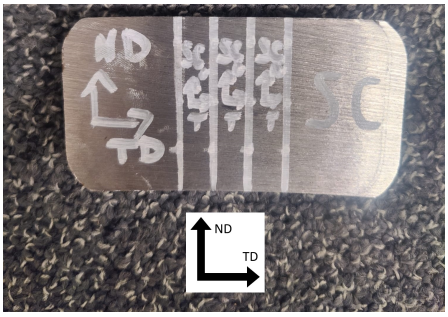

(b) Samples Extraction Samples A,B,C

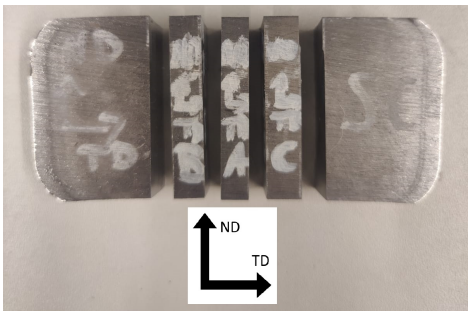

(c) Samples Extraction Samples A,B,C

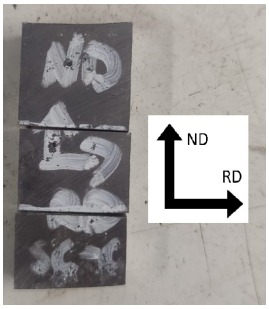

(d) Sample Extraction Samples U,M,L

Figure 3.2: Overview of samples Extraction: a) Initial samples removed from the trailing arm. b) and c) Locations of where samples A, B and C were taken from each sample. d) How each sample was further subdivided into an upper (U), middle (M), and lower (L) section.

the results of this analysis.

Sanding, Polishing and Etching

In order to prepare the samples for the experimental steps of the research, sanding, polishing and etching steps are required to ensure high-quality results.

Table 3.3: Overview of the sanding process used for the 51Crv4 samples throughout this research.

Grit	Rotation Speed (rpm)	Time (s)
P80	250	120
P180	250	120
P320	250	120
P800	250	120
P1200	250	120
P2000	250	180

The initial stage of sample preparation for testing is sanding. Due to the sample size requirements of the EPMA and SEM machines, the majority of samples were prepared without the use of mounting resin. Sanding was done using the n Struers LaboPol-25. The sanding process was done as seen in table 3.3. Each sanding step was done until no scratches from the previous step remained. This results in the approximate time seen in the table. Typically the final stages took longer due to the smaller scratches being more difficult to remove.

Following the sanding steps, the samples were polished using 3µm and 1µm polishing agents. Both polishing steps were done using a Struers polishing machine. The 3µm polishing step was done using

a MD-nap polishing cloth whilst the 1µm step was done using a MD-mol polishing cloth. Both steps were done using a rotation speed of 300 rpm for approximately 5 minutes. This time is an estimate and the samples were checked for scratches using an optical microscope throughout.

For certain steps of the research, a clear view of the microstructure is required. Therefore an etching stage is required. Etching was done using Nital 2% and requires an application time of 15 seconds. This was consistent across the sample from the different manufacturers. Due to the high oxidation rate of the 51CrV4 steel, the samples often required re-etching. This requires the removal of the oxidized layer which can be achieved through the final sanding step at grit P2000. All subsequent steps of the sample preparation process are therefore also required before re-etching.

3.2. Microscopy

Figure 3.3: Keyence VHX-5000 digital microscope used during microscope analysis.

Microscope analysis was done using a Keyence VHX-500 microscope. In order to properly view the bands, which run parallel to the rolling direction, the samples were orientated in such a way to view the transverse direction face (ND-RD plane). This orientation can most clearly be seen in figure 2.11 in the background section. Microscopy was done using the U, M and L sub-samples for samples A, B and C for all four of the steel products. Microscopy is used to confirm the presence of carbide band formation in the trailing arms and to confirm that the manufacturing steps undergone by the trailing arms result in roughly the same microstructures. Furthermore, microscopy is necessary to get an initial understanding of how the carbide band formation develops throughout the depth of the samples. As well as which other microstructural constituents form and how they develop as a function of surface depth.

3.3. Segregation

3.3.1. Micro-Segregation

Electron Probe Micro-Analysis (EPMA) is done to characterize the underlying chemical banding present in the material. This is done by determining the local concentration of alloying elements throughout the surface of the sample. This chemical banding is one of the primary causes of microstructural banding and will help us to understand the nature of the banding present in the material. EPMA was done on samples from both the upper (U) and middle (M) parts of the suspension arm in sample A from all four of the steel products. Measurements were taken at three different depths, namely, at the surface, 25%

from the surface and at the center of the sample. At each depth, measurements were taken across a depth of 1 mm with a measurement step size of 10µm. From this, the level of micro-segregation can be determined at the different depths as well as the average micro-segregation spacing. This will provide insight into the underlying causes of the carbide band formation.

3.3.2. Macro-Segregation

Macro-segregation was measured using the energy dispersive X-ray spectroscopy (EDS) function from the JEOL JSM-IT100 seen in figure 3.4. Area measurements were made on images with a magnification between 50-200x. Magnification ranged slightly due to these measurements often being made in conjunction with other EDS and scanning electron microscope (SEM) experimental data. Measurements were made over the entire area of the SEM images being analyzed in order to avoid inaccurate data due to local micro-segregation peaks. Furthermore, measurement spacing and depth differed somewhat across the different steel products due to measurements being time-limited and overlapping in analysis where the SEM was used. However, for all samples measurements were taken from the surface to the center of the samples with a maximum measurement spacing of 11%.

Figure 3.4: Jeol JSM-IT100 scanning electron microscope (SEM) used during analysis. This machine was also used for energy dispersive X-ray spectroscopy (EDS) results.

3.4. Hardness

Hardness testing was done using Vicker's hardness measuring method. The hardness testing was done using a Struers Emco-Test DuraScan automatic hardness tester similar to the one seen in figure 3.5. Hardness tests were done in two manners. The first hardness tests were done to determine the effect of surface depth on the local hardness. These tests were done using samples that were fully sanded and polished but not etched. This was done to improve the accuracy of the measurements. The measurements were done at ten depths from the surface, ranging from near the surface to the center of the sample. The measurement depth was equally spaced and for each depth 10 measurements were made. These measurements will therefore give a good indication of how the hardness is affected by the depth, as well as the expected hardness range at each depth. These measurements were made using the HV 2 method in order to achieve a larger indent and have a better understanding of the overall hardness in the region of the sample.

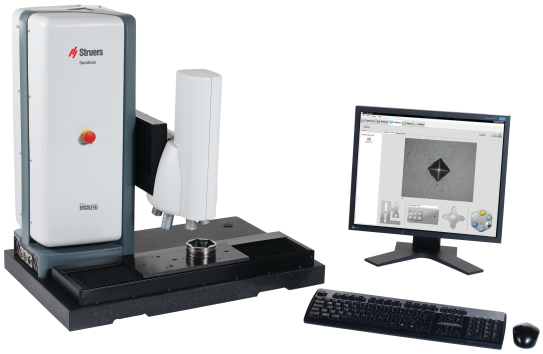

Figure 3.5: Struers Emco-Test DuraScan automatic hardness tester used during hardness analysis.

Further hardness tests were done extensively on the microstructural bands present in the sample. This is done to create a clear statistical analysis of the band properties and helps us understand the nature of the banding. Individual properties of microstructural bands help give an indication of the different forms of banding present in the microstructure. Hardness tests were done on samples from both the upper (U) and middle (M) parts of the suspension arm. For each location hardness tests were conducted for all three individual samples A, B and C across all the steel products. This testing was done using the same hardness testing machine as the previous testing which can be seen in figure 3.5. Vicker's testing method for the band hardness testing was smaller than the previous hardness testing method. A smaller indent force was used to ensure indents were smaller than the band width and therefore the HV 0.2 method was used.

3.5. Phase Fraction

Phase fraction was determined using X-ray diffraction (XRD). The XRD used was a Bruker D8 Advance diffractometer BraggBrentano geometry with graphite monochromator and Vantec position sensitive detector with the use of cobalt radiation (λ = 1.79 Å). The XRD analysis will help us understand the phase fraction of carbides present in the material as well as the other phases present in the material. This will help to give a baseline in the level of carbide band formation which could occur in the microstructure.

3.6. Band Area

Band area analysis was done using a scanning electron microscope (SEM), namely the EOL JSM-IT100 seen in figure 3.4. Previously this device was also used for the macro-segregation analysis. This analysis was done by determining the grey scale of the SEM images of the different samples at differing depths in the microstructure. With the use of the grey scale figure, it is possible to separate the area fraction of the carbide banded region from the other regions in the microstructure. This process can be seen in figure A.9 in the appendix. By determining the peak caused by the non-carbide banded microstructural constituents and removing this from the overall curve, the peak caused by the carbide bands can be determined. From this, the area fraction can be determined. This process was done using the upper (U) and middle (M) sample B from all the different steel products. The maximum measurement spacing was 7% of the sample thickness or approximately 2.5mm. A minimum of three measurements were made at each depth to ensure reliability of the results.

3.7. Band Composition

Band composition was analyzed using EDS analysis similar to what was done for the macro-segregation analysis. Therefore this analysis was also done using the JSM-IT100 seen in figure 3.4. To determine the band composition, the EDS analysis was focused on the carbide banded regions rather than large areas of the microstructure. From this, the concentration of alloying elements can be determined for individual bands. This will help determine which elements are predominately present in these regions and how the concentration of alloying elements in the carbide region develops in relation to the surface depth. This analysis was done in 4 or 5 different locations of sample B for each steel product, with 5-8 measurements being made at each location across many carbide bands. The measurements were taken at varying depths where there was clear carbide band formation. This will help us understand how the carbide band composition tends to differ across the carbide banded regions as well as how this may differ as a function of depth.

4

Results

4.1. Previous Results

Previous research was done by Lie Zhao at VDL Weweler to understand the types of carbides which form in 51CrV4 Steel. This was done by simulating the heat treatments using Thermocalc software. The results can be seen in table 4.1. From this, it would be expected that the M3C carbide will be most predominantly present in the microstructure with a smaller fraction of M7C3 and MC carbides.

Table 4.1: Overview of the Carbides which form in 51CrV4 steel, the composition, crystal structure, and the maximum fraction which can be found in the steel according to Thermocalc simulations.

Carbide Type	Composition	Crystal Structure	Max. Fraction
M3C	Fe, Cr, V, Mn	Orthorhombic	6.58%
M7C3	Fe, Cr, Mn	Orthorhombic	2.61%
MC	Fe, Cr, Mn, V	FCC	1.94%

4.2. Microscopy

In order to understand the carbide band formation in the 51CrV4 and how this differs across steel from different manufacturers, it is important to have an understanding of the microstructure and how it develops across the surface depth. Additionally, this analysis will help give an initial indication of how the carbide band behavior differs across the different steel samples. The trailing arms underwent a final quench and temper heat treatment to achieve a primarily martensitic microstructure. Due to the heat transfer process of the trailing arms, the region near the surface experiences a much higher cooling rate compared to the region near the center. This should result in a much higher fraction of martensite near the surface.

The microstructural analysis revealed that there are three main microstructural regions, a tempered martensitic region, a banded carbide region and a region of several softer microstructural constituents. These regions can be seen in figure 4.1.

The main microstructural regions found across the four steel samples can be seen in figure 4.1. The most predominant microstructure is the tempered martensitic microstructure seen in figure 4.1a. The carbide band microstructure which is the focus of this research can be seen as the lighter phase in figure 4.1b. Finally, the third microstructural region which can be seen in the 51CrV4 samples is a microstructure that consists of ferrite, pearlite as well as other softer microstructural constituents seen in

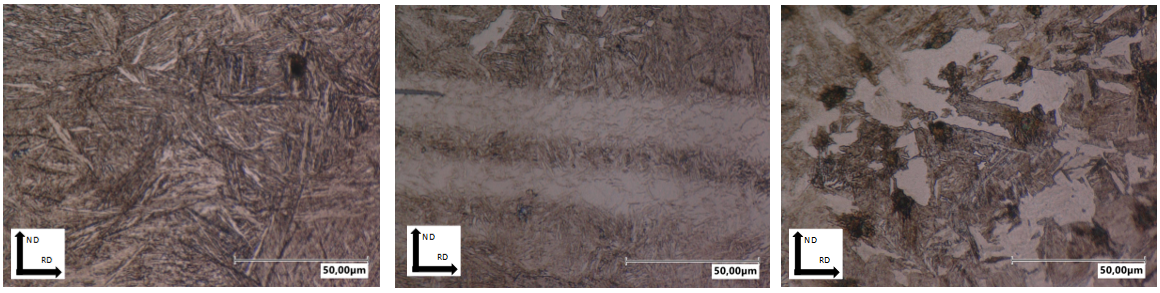

(a) Tempered Martensitic Microstructure (b) Carbide Band Microstructure (c) softer microstructural constituents

Figure 4.1: Overview of the different microstructural regions found in the 51CrV4 steel samples. Three main microstructural regions can be found. In figure 4.1a the primarily martensitic microstructure can be seen. In figure 4.1b the carbide banded microstructure can be seen. In figure 4.1c a microstructure of ferrite, pearlite and other microstructures can be seen.

figure 4.1c. Towards the surface, the microstructure consists of a nearly fully tempered martensitic microstructure. Towards the center, the fraction of the softer microstructural region gradually increases as a function of the surface depth. Furthermore, the carbide banding phase tends to initially form around 20% from the surface and gradually increases towards the center. The carbide banding microstructure becomes more distinct towards the center which would indicate that the carbide fraction in these regions is likely higher. The softer microstructural constituents tend to form between regions where hard carbide bands are predominantly present. The formation of the softer microstructural constituents occurs more closely to the surface than the carbide bands and is thus not directly related to the carbide band formation. The manner in which the microstructure develops as a function of surface depth is quite similar across the four samples from different manufacturers. The aforementioned microstructural regions can be found in all four samples, with no other significant microstructural regions being found. The fraction of each microstructural region as well as the manner in which it develops across the surface depth does differ somewhat across the samples. This research focuses on the carbide banding microstructure. Therefore, how the tempered martensite and softer microstructural constituents develop across the sample will not be analyzed. How the banding microstructure develops will be analyzed in two ways; The carbide start depth will be analyzed using the microscope images and can be seen in table 4.2; How the carbide band area develops will also be analyzed using SEM images and has been introduced in subsection 3.6.

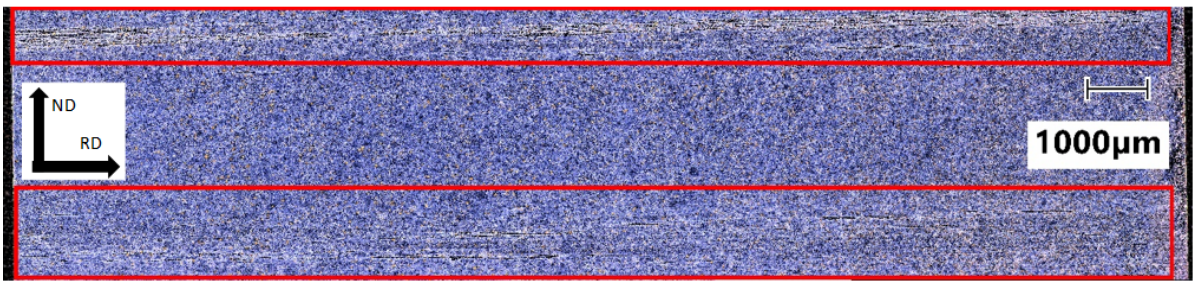

Figure 4.2: Example of heavily carbide banded regions found in sample SK-B. The carbide banded regions are indicated by the red rectangle. The area between the carbide bands is much larger than what is found in other parts of the sample. Moreover, it contains significantly fewer carbide bands.

One important note on the formation of carbide banded microstructure that was noticed during microscope analysis is that the development of the carbide banding regions is not always consistent and that often regions of very dense carbide formation can occur surrounded by a larger region with little carbide formation. One clear example of this is in the sample SK-B which can be seen in figure 4.2. These regions are expected to have a significant impact on the mechanical properties and will be discussed further in the 4.3.

In table 4.2 the depth at which carbide band formation starts can be seen. Overall, very clear differences can be seen across the samples. Even across samples from the same manufacturers there is a slight

Table 4.2: The depth from the surface at which carbide band formation begins for all the samples. The depth is given as a percentage of the total thickness of the sample.

	KG	SC	SK	SL
Sample A:	18.1%	25.4%	22.9%	16.3%
Sample B:	17.0%	24.2%	21.8%	15.4%
Sample C:	18.6%	25.9%	20.2%	17.9%
Average:	18.2% (+/- 0.9)	25.2% (+/- 0.9)	21.7% (+/- 1.4)	16.6% (+/- 1.3)

difference in carbide band start depth. This is due to a variety of reasons, the most notable of which is that band formation is usually limited at the depth at which it starts. This means carbide bands are not as clearly seen in the microstructure which leads to inconsistencies in where the first bands are seen. The SL samples have the earliest band formation across all samples with an average band start depth of 16.6%. Band formation in the KG and SK samples occurs at a slightly greater depth compared to the SL sample at 18.2% and 21.7%. Band formation occurs deepest in the SC sample at 25.2%. These results would indicate that the SC sample has the best carbide banding behavior for trailing arms. This is because trailing arms are loaded with bending stresses which leads to the greatest stresses occurring near the surface of the trailing arm. Therefore, the SL and to a lesser extent KG samples would be most impacted by the carbide band formation in the microstructure.

4.3. Hardness

The micro-hardness testing has been used to understand the impact of the carbide band formation and the other microstructures present. This has been done in different manners in order best understand the effect of carbide bands. The first type of hardness tests done were to analyze how the hardness develops as a function of the surface depth. As mentioned in section 4.2, the surface consists primarily of tempered martensite with the carbide microstructure, as well as other softer microstructures, becoming more gradually present towards the center. The carbide microstructure is expected to have a higher hardness than the other microstructures present, and therefore its impact should be clearly seen in the hardness tests. This test will therefore help in understanding how the carbide bands and other microstructures develop with the surface depth.

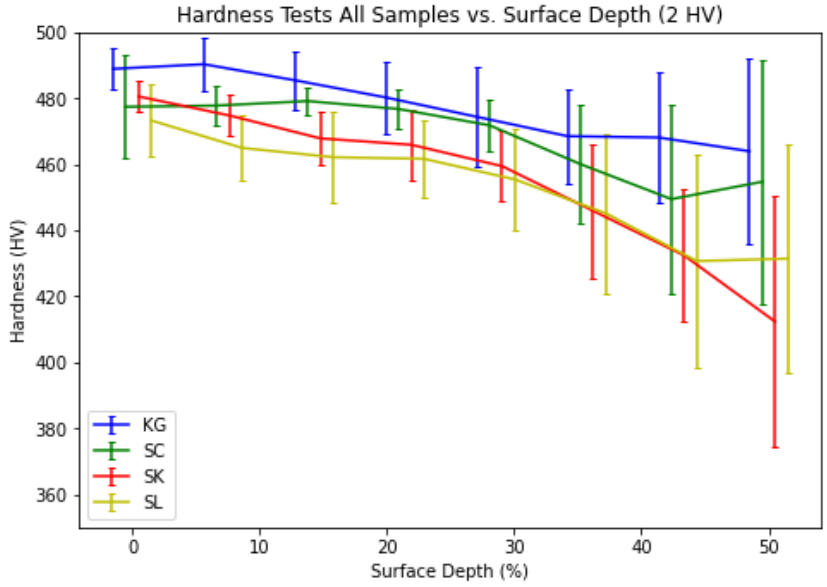

Figure 4.3: Overview of how the Vickers hardness develops as a function of the surface depth. Results are shown for steel from all four manufacturers. Results are based on the average hardness across the three samples from each manufacturer. The results for each individual sample can be seen in figure A.2 in the appendix.

In figure 4.3 the hardness vs. depth relation can be seen for the steel from each manufacturer. These measurements were done using each sample (A, B, C) and done using the U and M sub-samples. This figure is based on the average of the three samples for all the manufacturers. Therefore the measurements were taken from the upper half of the trailing arms. There are two main trends to note from these figures.

Firstly, the hardness relationship for all of the steel samples is higher at the surface and subsequently lower in the middle. There are several factors influencing these relations. Most notably as discussed earlier, is the lower cooling rates that occur towards the center of the trailing arms due to being cooled from the surface. This results in a somewhat different microstructure at the center compared to the surface. At the surface, the samples are expected to be fully martensitic. This corresponds well with our measurements as the mean hardness is in the range of what would typically be expected for martensitic steel. Closer to the surface the microstructure is expected to be a combination of ferrite and martensite. This helps explain the reduced hardness in the center of the samples.

The second trend that can be seen in the figure is the increased standard deviation that occurs towards the center of the sample. This factor is in large part due to the aforementioned presence of a dual-phased microstructure in the center of the sample compared to the single-phase microstructure at the surface. The peaks in hardness, however, can often be seen to be higher at the center than at the surface. This is best explained by the presence of significant carbide regions in the microstructure, as carbides are even harder than martensite. A significant carbide presence would be enough to counteract the softer ferrite and lead to higher hardness measurement.

The presence of banded microstructure would also help explain why the reduction in hardness is not always a smooth relation and why there are noticeable differences for samples from the same manufacturer. Banding typically follows the rolling direction and as such, measurements taken at a similar depth are expected to experience a similar amount of banding. Therefore if a hardness measurement coincides with a carbide banded region, then the other measurements taken at that depth are expected to coincide with the carbide banded region. The same can be said for measurements taken in the ferrite-banded regions. One clear example of this is in figure A.2b where sample B has a much higher hardness at the center of the sample compared to samples A and C. As mentioned in section 4.2 sample SK-B has a significantly carbide banded region in the center of the sample, this banded region is likely the cause of the increased hardness at the center of this sample.

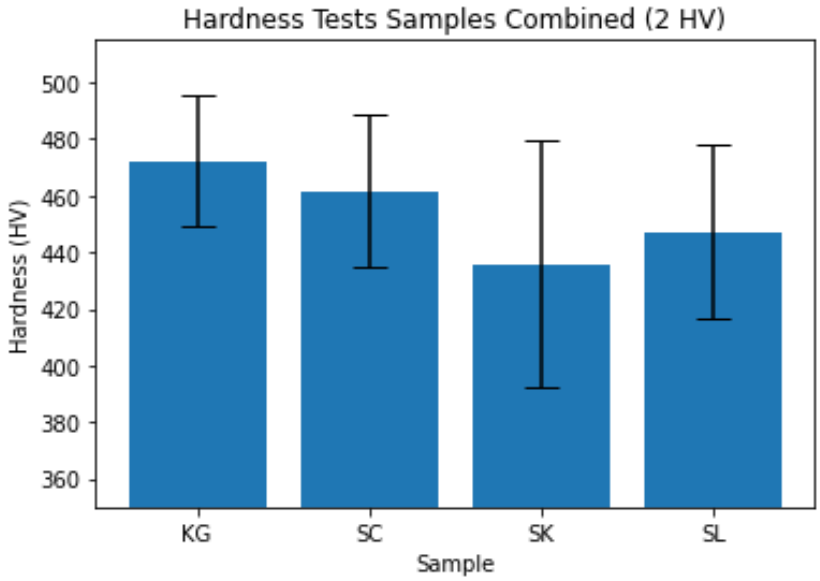

Figure 4.4: Overview of the average hardness (Over samples A, B and C) for the samples from all the manufacturers. The standard deviation for each sample is also indicated in the figure. These results are based on the hardness measured for each individual sample which can be seen in figure A.1 in the appendix.

The hardness tests used in figure 4.3 can also be used to understand how the overall hardness of the samples compares. These results can be seen in figure 4.4. It can be seen that the KG samples have the highest overall hardness and the SK samples have the lowest overall hardness. As mentioned earlier it is unclear if this is due to the carbide band fraction or the presence of softer microstructural constituents.

Next to the hardness tests done to analyze the hardness vs. surface depth relation, hardness testing on the carbide bands was also done. This was done to analyze the range of hardness in these carbide bands as well as how this differs across samples from different manufacturers. This will also help indicate the density of carbides present in the carbide banded regions, as a greater hardness in these regions indicates a greater presence of the harder carbides. The results of this analysis can be seen in figure 4.5. These measurements were based on the measurements of all three samples for each manufacturer, the measurements for each individual sample can be seen in the appendix in figure A.3.

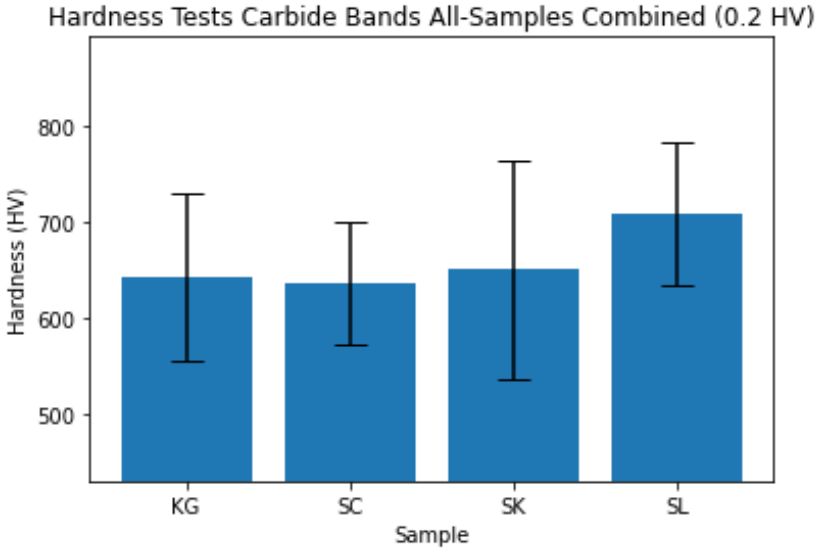

Figure 4.5: Overview of the average hardness in the carbide banded region for the samples from all the manufacturers. The standard deviation for each sample is also indicated in the figure. These results are based on the hardness measured for each individual sample which can be seen in figure A.3 in the appendix.

In figure 4.5 the average hardness for the carbide banded region for the samples from each manufacturer can be seen. The SL samples have the greatest average hardness, this indicates that the carbide in the SL sample has a higher density in the carbide banded region. Furthermore, the other samples have a very similar average carbide band hardness, indicating that the carbide density is likely very similar in these samples. It is important to note that the standard deviation in the SK samples is somewhat higher compared to the other samples. As can be seen in figure A.3 this is primarily due to a significant difference in carbide band hardness across the three samples and primarily in sample SK-B. As mentioned in subsection 4.2 the SK-B sample has regions where carbide bands are more abundant than what is seen in other parts of the microstructure and the other samples. These regions are likely the reason that carbide band hardness is higher in sample SK-B and why the standard deviation is greater across the SK samples.

4.4. X-Ray Diffraction

X-Ray Diffraction (XRD) analysis was done to understand the concentration of phases present in the 51CrV4 steel samples. The XRD analysis can be seen in the appendix in figure A.4. The resulting phase fractions can be seen in figure 4.3. Due to significant overlap in XRD peaks expected for the different M3C carbide microstructures (which include cementite), they were all referenced into the same phase concentration, namely, that of cementite. The M7C3 carbides have a similar orthorhombic crystal

structure as the M3C, because of this M73C carbides are likely incorporated in the cementite phase fraction. It can be seen that the remaining microstructure is almost entirely Alpha or BCC, this fraction includes the tempered martensite present in the material. A small concentration of 1% FCC is also present within the material. As seen in table 4.1, a small fraction of MC carbides are expected to be present in the microstructure. These carbides have the FCC microstructure, this would help explain the small fraction of FCC found, however, a fraction of retained austenite could also cause this small fraction. The 7% phase fraction of FCC and Cementite phase in table 4.3 would therefore likely indicate the upper limit on the carbide fraction present in the material. This corresponds well with what was found in table 4.1. The final phase fraction of carbides is expected to be lower than this 7% upper limit as other microstructures such as cementite and retained austenite are likely present.

Table 4.3: Overview of the phase fractions present in the 51CrV4 steel samples from XRD analysis.

Phase	Fraction (+/- error)
BCC	0.93 +/- 0.001
FCC	0.01 +/- 0.0003
Cementite	0.06 +/- 0.001

4.5. Band Area

As mentioned previously, the mechanical effects of carbide band formation on the trailing arms is highly dependent on the location of the carbide bands in the material. Trailing arms experience bending stress and therefore the mechanical properties of the material at the surface are most critical to the performance of the trailing arm. It is therefore important to analyze how the carbide banding differs as a function of the surface depth. This was done using the SEM. Measurements were taken at differing depths for each material. The first measurements were taken at 0.5mm from the surface and subsequent measurement spacing was 2.5mm per measurement. At each depth between 3-5 measurements were taken for each material. The carbide band area was measured using the SEM. Further processing was done using Image J software. The SEM images were taken at 200x zoom, this was done to maximize the image area to improve analysis whilst not dealing with coloration issues that come at lower magnification levels. The carbide band area was determined using the grey-scale analysis in the Image J software from which the carbide band peaks could be extracted from the background peak to determine the carbide band area. This process is explained in more detail in the appendix in figure 3.4. The results of this research can be seen in figure 4.6.

As observed before, from the microstructural characterization using light optical microscopy the carbide band formation tends to start at differing depths for the samples. This can also be clearly seen in figure 4.6. The carbide band fraction is around 0% for the first 20% of the surface depth. After which the SL sample shows the earliest increase in carbide band fraction towards the center at just over 20%. The other samples seem to show the carbide band fraction increased most significantly at approximately 30%. There is also a clear difference in the way the carbide fraction is built up across the surface depth for the different samples. The SL and SC samples show a more abrupt increase and subsequent plateau towards the center, this behavior is most prevalent in the SC sample. Whilst, the SK and KG samples have a more gradual increase in carbide fraction with the ultimate peak occurring more towards the center. Overall, SL and SK samples have the highest carbide band fraction towards the center. It is important to note that the SL samples carbide band fraction is highest between 30-40% and subsequently decreases towards the center. This is more likely due to the limited sample size of the results rather than any underlying microstructural characteristic. Figure 4.6 is useful in determining how the carbide band fraction is built up across the 4 samples, however, it does not give the best indication of the overall level of banding occurring in the samples. Therefore, it is also important to see what the overall band fraction in the samples is. This can be done using the same raw data. The resulting average carbide band fraction can be seen in table 4.4.

As seen in table 4.4 the overall band fraction is highest in the SL sample and lowest in the KG sample. The higher carbide band fraction in the SL sample is a result of the carbide band formation occurring

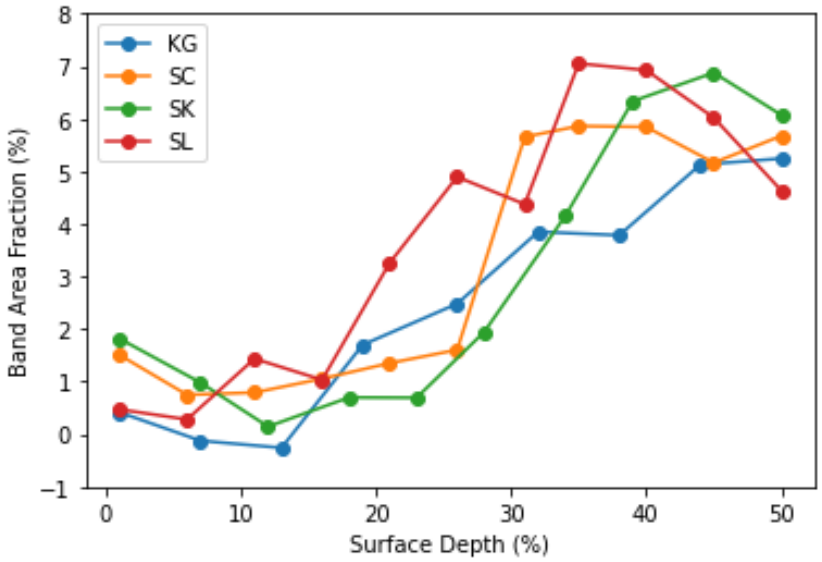

Figure 4.6: Overview of how the carbide band area differs relative to the surface depth. The carbide band area was measured at differing depths for all the samples. The carbide area increases towards the center of the sample. This increase is built up and to what extent this happens differs significantly across the samples. Band area measurments have an uncertainty of +/- 2%

Table 4.4: Average Carbide Band Area Fraction based on the SEM results from figure 4.6.

Manufacturer	Carbide Band Area Fraction (%)
KG:	2.47
SC:	2.96
SK:	2.97
SL:	3.57

closer to the surface compared to the other samples as seen in figure 4.6. The carbide band formation occurs much later and is more gradual in the KG sample compared to the other samples this explains why it has a lower average band area fraction. The overall band area fraction of the SC and SK samples are very similar, however, the build-up of the carbide fraction differs slightly between these samples. As seen in figure 4.6 the SK sample has a more gradual increase of band area towards the center, however, achieves a greater carbide band fraction towards the center. Whilst the SC sample has a steep increase of carbide band fraction at approximately 30% followed by a subsequent plateau.

The differences in band formation can be clearly seen in these results as well as the results from previous sections. It is however also important to understand the underlying microstructural parameters which lead to carbide band formation and how they differ. This will help us understand what causes the differences in carbide band formation and which steel grade has the best properties.

4.6. Segregation

As mentioned in chapter 2 segregation is the occurrence in which the local chemical composition in steel differs at different locations in the steel. The level of segregation can be best defined by the local alloy concentration over the average alloy concentration in the material. This difference in chemical composition can significantly impact the steel in terms of microstructural characteristics as well as mechanical properties. Segregation is typically characterized in two ways, namely, micro-segregation and macro-segregation. Micro-segregation is very local chemical concentration peaks within the steel which cause favorable conditions for microstructures to nucleate. The microstructures that form in these regions are dependent on whether the local elements are more predominately ferrite or austenite stabilizing. Macro-segregation is more global in terms of the steel component. This can have a significant

impact on the microstructures that form throughout the material. It has little effect on the local banding behavior of the steel compared to micro-segregation, however. Both types of segregation were investigated during this research. The micro-segregation was researched using electron probe micro-analysis (EPMA) results and the macro-segregation was researched using EPMA and EDS results.

4.6.1. Micro-Segregation

As mentioned in chapter 2, band formation is typically correlated to the micro-segregation present in the material. Micro-segregation is typically characterized using two parameters, namely, the micro-segregation spacing and micro-segregation peak value. Micro-segregation spacing is important to consider as when the spacing is too large the carbon atoms in the lattice are not able to diffuse the distance necessary to create the favorable nucleation sites which leads to band formation. Likewise, if the micro-segregation spacing is too small the formation of a clear banded region will be limited due to an overabundance of nucleation sites. Furthermore, the micro-segregation peak value is important to consider as a certain amount of segregation is necessary to create thermodynamically favorable location sites. These two parameters will be the focus of the micro-segregation analysis. The micro-segregation was analyzed using EPMA. Steel samples from each manufacturer were analyzed at three depths, namely, at the surface, 25% from the surface and at the center of the sample. The measurements were carried out over a distance of 1mm with a measurement step size of 10 µm. Using EPMA results, the local chemical concentration can be seen and from this, the micro-segregation peaks can be determined. From this, the micro-segregation spacing and peak level can be determined and compared for the 4 different samples. This will help to understand the microscopy and SEM results. The raw data of the EPMA results can be seen in the appendix.

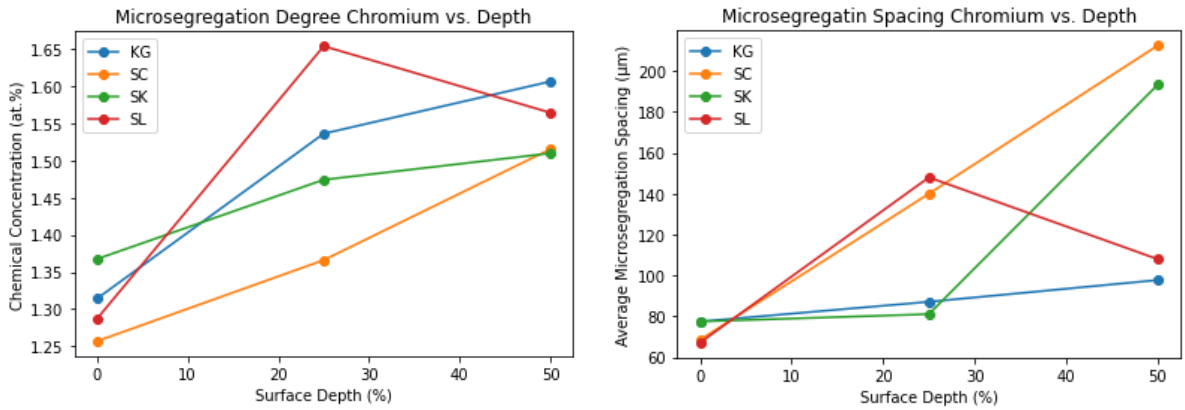

(a) (b)

Figure 4.7: EPMA analysis of the results seen in the appendix. The 4.7a) micro-segregation peak segregation and 4.7b) micro-segregation spacing has been compared for all four samples as a function of the surface depth. Peak locations were determined using a python code with peak height and width filters to ensure no peaks were measured twice. This was followed by visual confirmation. The microsegregation degree measurements have a standard deviation up to 0.3% chemical concentration, whilst, the micro-segregation spacing has a standard deviation up to 100µm.

As discussed in chapter 2 previous research has found that micro-segregation typically increases as a function of surface depth due to increasing inter-dendritic spacing that occurs towards the center of slabs. This behavior can also be seen in all the 51CrV4 samples as seen in figure 4.7b. There are significant differences in how the micro-segregation spacing develops as a function of depth for the different samples. The SC sample exhibits the type of behavior which would have been expected on the basis of literature, in which the micro-segregation spacing increases gradually as a function of depth. The behavior of the KG also exhibits a behavior similar to what is expected in literature, however, the rate of increase in micro-segregation spacing is much lower. This difference indicates that there are significant differences in the solidification processes undergone by the different steel manufacturers. The SK and SL samples show very different behaviors in terms of micro-segregation spacing. The SK samples initially show a flat relation which significantly increases towards the center. Whilst, the SL

samples initially show a steep increase followed by a slight decrease in micro-segregation spacing. The large internal changes in micro-segregation spacing are likely a function of the solidification mechanics differing at different depths of the initial slab as mentioned in chapter 2 and seen in figure 2.2.

In figure 4.7a the average peak concentration of chromium can be seen. This value is typically heavily linked to the band formation in steels as a certain amount of micro-segregation is necessary for bands to form. If the micro-segregation is not significant enough, then the bands are unlikely to form as these locations do not have the thermodynamic favorability that is required. In 4.7a it can be seen that the chromium concentration in the peaks is very similar for all the samples at both the surface and center of the samples. The concentration is substantially greater at the center compared to the surface. This is as expected since for all the samples no carbide band formation occurs towards the surface. Furthermore, all the samples experience clear carbide band formation as seen in both the microscopical analysis and the band area analysis.

Where the chromium peak concentration differs most significantly across the samples is in the measurements taken at 25% from the surface. The SL sample has the greatest micro-segregation, followed by the KG and SK samples. The SC sample has a significantly lower micro-segregation at 25% from the surface. Overall, for most of the samples, there is a greater increase in micro-segregation from the surface to 25% from the surface compared to 25% from the surface to the center. This behavior is slightly different from what was found in literature as seen in figure 2.5. From this figure, it would be expected that the segregation intensity would increase more significantly towards the surface. However, the investigation shows a greater increase in segregation intensity near the surface.

If the micro-segregation intensity is compared to the microscopy and the band area analysis we can see a clear trend between the micro-segregation intensity and the band formation. As seen in section 4.2 the band formation in sample SL occurs at an earlier stage than the other samples, whilst the band area analysis in section 3.6 indicates that the carbide band fraction at 25% from the surface is much greater in the SL sample compared to the other samples. The KG and SK samples have similar behavior for micro-segregation intensity and this is very similar to what was seen for the carbide band start depth and band area analysis. Carbide formation occurs slightly earlier for the KG sample and the carbide area fraction is somewhat higher at 25% from the surface. This all relates well to figure 4.7a as the micro-segregation peak for the KG sample is also slightly higher. The SC sample has the lowest micro-segregation intensity and this again corresponds well with previous results. 25% from the surface is also where the carbide band formation tends to start for the SC sample. This could indicate that the micro-segregation intensity measured for the SC sample at 25% from the surface is the minimal segregation intensity necessary for carbide band formation to occur. A more thorough EPMA analysis would be required to confirm this. Furthermore, a more thorough EPMA analysis would help compare these results to the band area measurements and thereby make the relationship between these two parameters more clear.

4.6.2. Macro-Segregation

As discussed earlier the macro-segregation does not have as significant an impact on banding behavior in steels. However, it is still an important aspect to understand. Typically the chemical concentration is greater towards the center compared to the surface. As mentioned in chapter 2, this is due to steel slabs solidifying from the surface towards the center. Macro-segregation can be investigated using both the EDS results as well as the EPMA results. The macro-segregation of chromium and manganese can be seen in figure 4.8 and figure 4.9. The macro-segregation of the remaining alloying elements can be found in the appendix in figure A.10.

In figure 4.8 the macro-segregation of chromium according to the EDS results can be seen. There is no clear macro-segregation relation present for the chromium phase. This is unexpected as literature research seen in chapter 2 found that a higher concentration of alloying elements would be expected towards the center. This likely indicates macro-segregation is less predominate in 51CrV4 steel compared to the steels used in the articles from the literature research. This same behavior is seen for

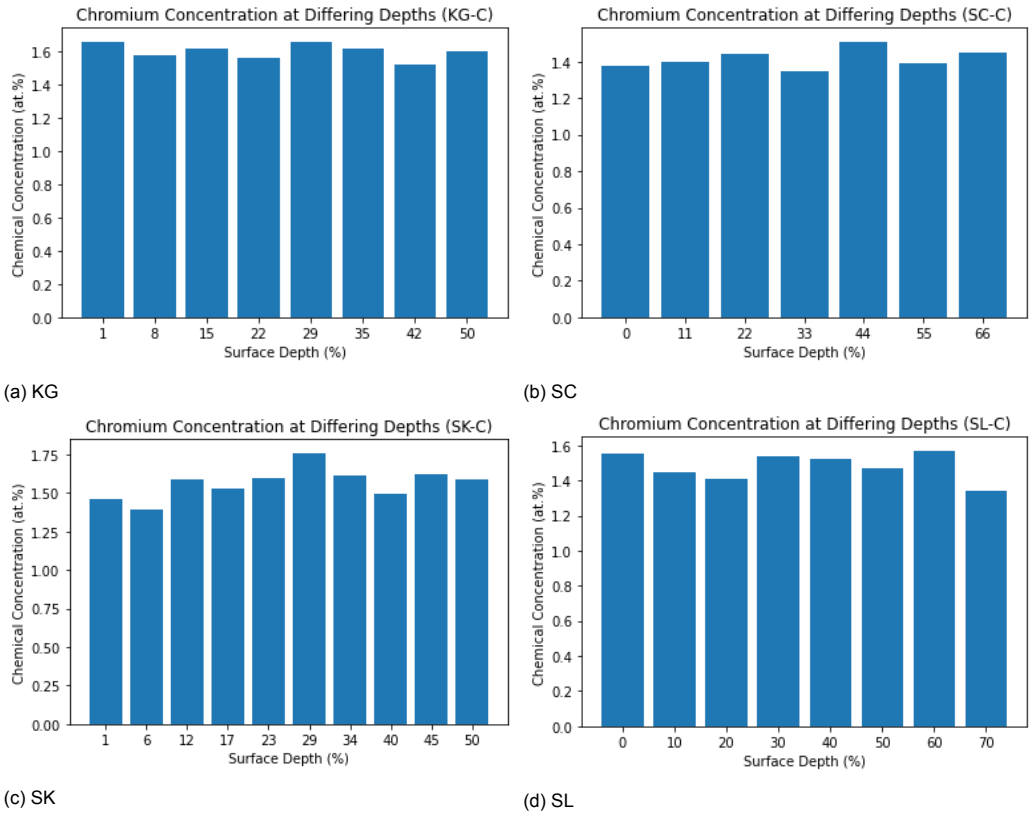

(a) KG (b) SC

(c) SK (d) SL

Figure 4.8: Overview of the micro-segregation of chromium present in the microstructure for the samples of all the manufacturers based on the EDS results. The figure that corresponds with each manufacturer is indicated in the sub-figure.

the manganese phase as seen in figure 4.9, as no clear macro-segregation can be seen. Finally, if we compare this to figure A.10, which contains all the alloying elements, significant variation in element concentration can be seen for the more minor alloying elements. However, there is no clear macro-segregation trend that can be seen and is more likely due to other effects.

Macro-segregation analysis could also be done with the EPMA results next to the EDS results. The macro-segregation from the EPMA results was based on the average of the measurements taken at every depth for the samples used. The results of this analysis can be seen in figure 4.10. These results indicate that there is no macro-segregation for the chromium, silicon and vanadium for all of the samples. Furthermore, there is no clear manganese macro-segregation for both the SC and SK samples. However, there is a small amount of manganese macro-segregation that occurs for both the KG and SL samples. The manganese macro-segregation that occurs for these samples can be most clearly seen from 25% from the surface to the center.

If we compare the macro-segregation results from the EDS and EPMA analysis it is interesting to see that the EPMA results indicate that there is a small amount of macro-segregation for manganese in both the KG and SL samples, whilst this is not the case in the EDS results. This likely indicates that the macro-segregation seen in the EPMA results is more due to a lack of sample size rather than any clear macro-segregation trend. This would best explain this inconsistency in the results as the EDS analysis give a more thorough analysis of the macro-segregation present in the samples. Furthermore, it is typically uncommon for macro-segregation to occur for one alloying element but not for any of the other alloying elements. Further EPMA analysis would be necessary to confirm if there is a clear macro-segregation trend for manganese in these samples or if this is due to the limited sample size.

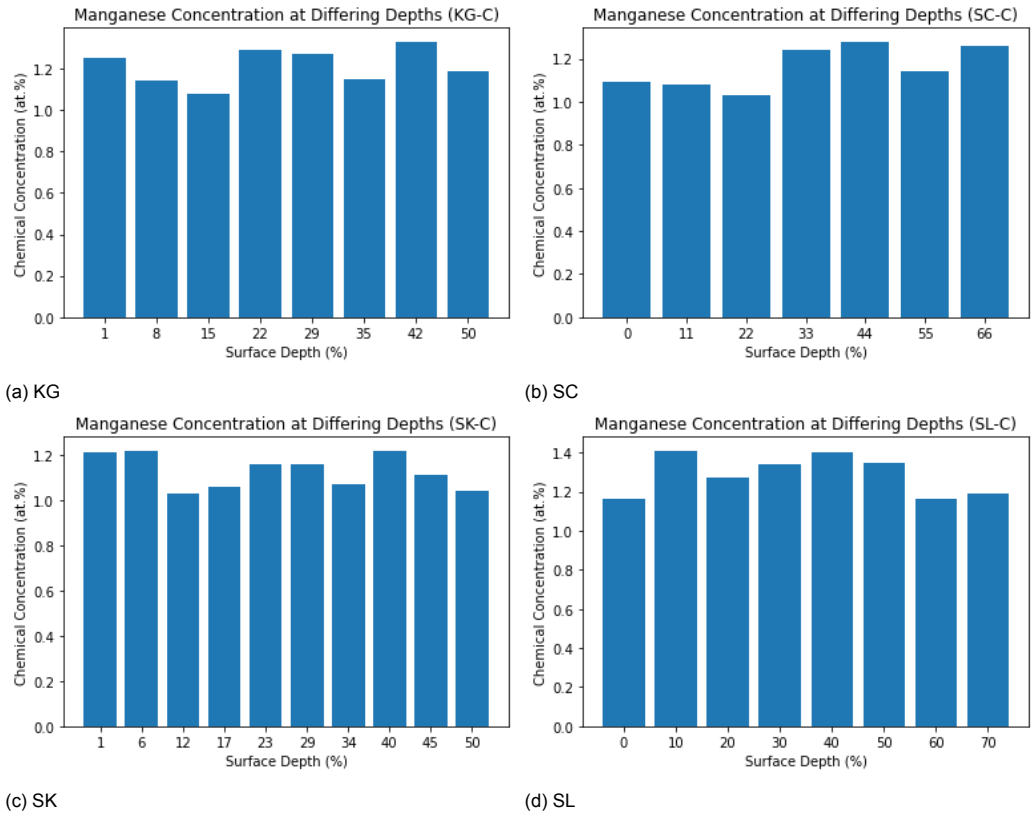

(a) KG (b) SC

(c) SK (d) SL

Figure 4.9: Overview of the micro-segregation of manganese present in the microstructure for the samples of all the manufacturers based on the EDS results. The figure that corresponds with each manufacturer is indicated in the sub-figure.

4.6.3. EDS Analysis Carbide Bands

EDS analysis was also done on the carbide banded regions to understand the chemical concentration of these regions, as well as if these regions remain consistent throughout the surface depth. These results can be seen in the appendix in figures A.11, A.12, A.13 and A.14. The chemical concentration of chromium is consistent in these regions and is well above what is found throughout the remaining microstructure. This would indicate that chromium carbides are heavily concentrated in these regions. Manganese also tends to be more abundant in these regions, however, the manganese concentration can differ quite significantly for different banded regions. Furthermore, the presence of large concentrations of manganese has been found to be heavily linked to the presence of an increased amount of sulfur as seen in the appendix in figure 4.11. This would indicate that manganese sulfides form in these regions. Vanadium has also been found to be more predominant in these regions. This could indicate that vanadium carbides also form in these regions. However, the chemical concentration of vanadium in these regions is inconsistent which would indicate that vanadium carbides are not a driving factor in the formation of these regions. Furthermore, the chemical concentration of vanadium overall in 51CrV4 steel is much lower than the chromium concentration and would therefore be less impactful on the chromium carbides.

The EDS analysis of the carbide bands also allows us to understand how the chemical concentration of the bands tends to develop as a function of the surface depth. These results can be seen in figure 4.12. There are substantial differences in the chemical concentrations in the different samples as a function of surface depth. For the KG sample, it can clearly be seen that the chemical concentration of chromium increases in the carbide banded regions towards the surface. This can also be seen to a somewhat lesser extent in the SK sample. However, the chromium concentration remains relatively consistent for the SC and SL samples towards the center. These results would help indicate why the formation of chromium carbide bands is more gradual in the KG and SK samples, whilst the SC and

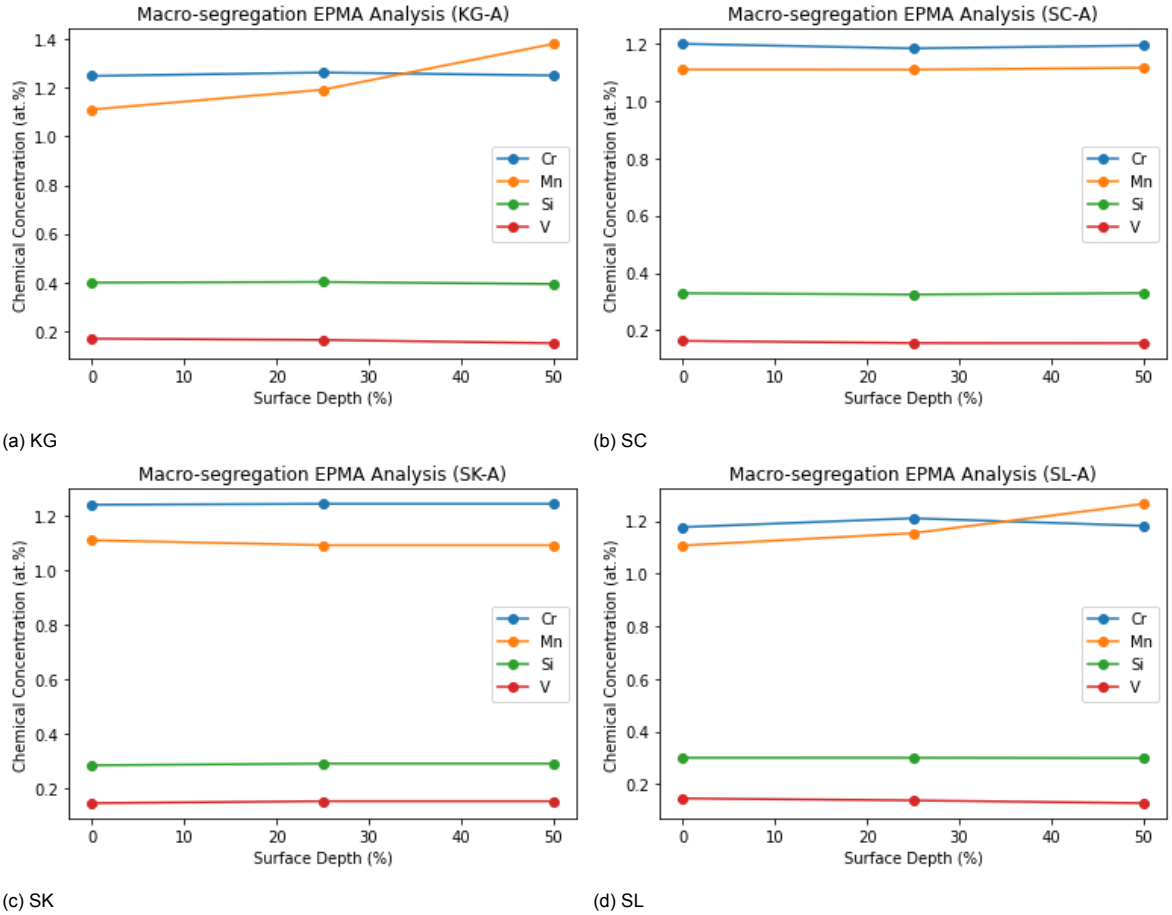

(a) KG (b) SC

(c) SK (d) SL

Figure 4.10: Overview of the micro-segregation of chromium, manganese, silicon and vanadium present in the microstructure for the samples of all the manufacturers from the EPMA results. The figure that corresponds with each manufacturer is indicated in the sub-figure.

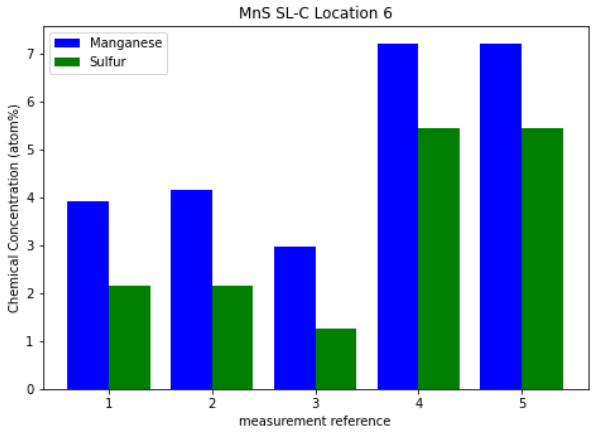

Figure 4.11: Example of the relationship between manganese and sulfur found in the 51CrV4 steel. This figure is from the SL sample.

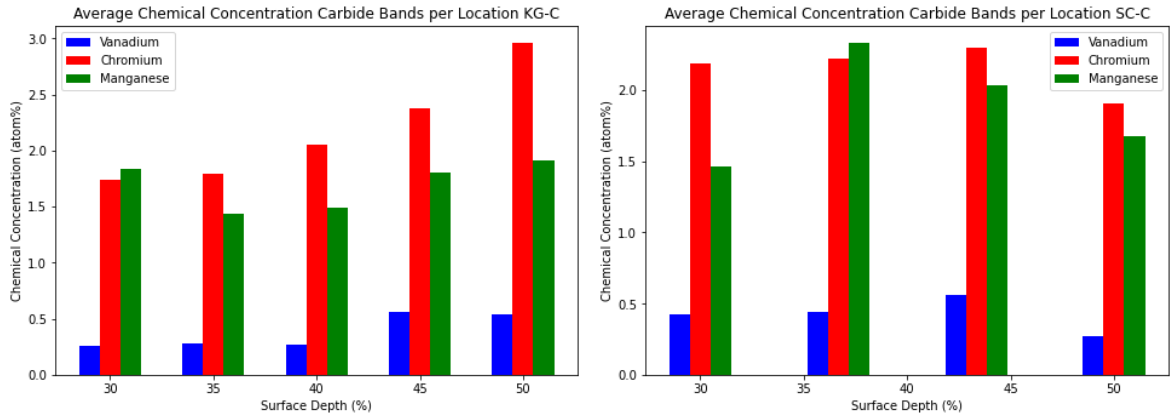

(a) KG

(b) SC

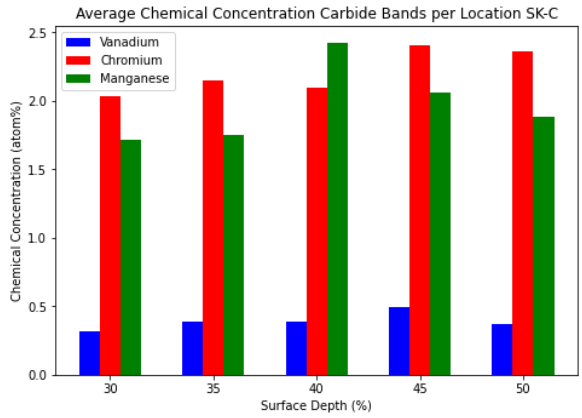

(c) SK

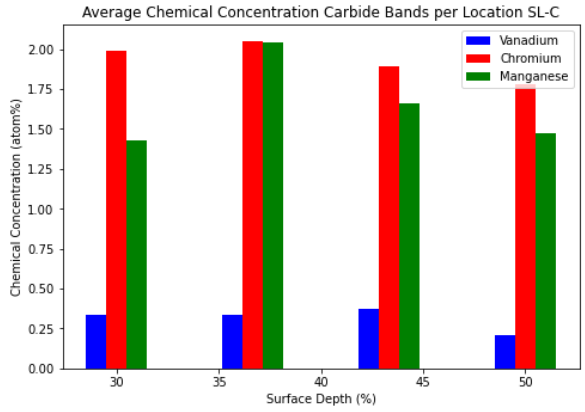

(d) SL

Figure 4.12: Overview of the carbide band element concentration as a function of depth from the surface for the four samples from different steel suppliers.

SL samples experience more of a plateau in terms of band area as seen in the band area analysis.

5

Discussion

The overall goal of this research was to understand the relation between the surface depth and band formation in 51CrV4 steel and how banding differs for 51CrV4 steel from different manufacturers. In order to reach this goal, many sub-research goals were set up. These were to correlate the surface depth to the formation of carbide bands, investigate the impact of the underlying segregation, identify the predominate banding microstructure, determine the banding start depth and identify the characteristics that lead to band formation. These goals were achieved with the use of microscopy, XRD, hardness, SEM and EPMA testing. This testing was done using 51CrV4 steel from four different manufacturers which were further processed by VDL using similar heat treatments and processing steps. The steel from the four manufacturers will be referred to as KG, SC, SK and SL. For the steel from each manufacturer, three samples were used from each manufacturer which were referenced as samples A, B and C.

The microscopy results indicated that the predominate microstructure at the surface was tempered martensite. Towards the center formation of carbide bands, as well as other softer microstructural constituents such as ferrite and pearlite, could be seen. These results also indicated that the band formation starts at differing depths as seen in table 4.2. From this, it could be seen that banding occurred closest to the surface for the SL and furthest from the surface for the SC sample. This indicates that the SC sample has the best banding behavior in this aspect as trailing arms are primarily loaded towards the surface. Therefore, band formation towards the center of the samples is less detrimental.

The hardness results, seen in figure A.2, indicates that the overall hardness reduces as a function of the surface depth. This is primarily due to the presence of the softer ferrite and pearlite microstructures towards the center. The standard deviation of the hardness measurements is also greater towards the surface as the presence of the harder carbide banding microstructure becomes more clearly present. Overall, the reduction in hardness towards the center is most significant for the SK sample and least significant for the KG sample. This is most likely due to an increase in the softer ferrite and pearlite phase towards the center being more significant in the SK sample than any carbide banding effects, as there is no clear impact on the band start depth to the hardness relation. Furthermore, the KG sample has the least overall sample thickness, indicating that the cooling rate in the center of the sample would likely be greater in the KG sample leading to a greater tempered martensite fraction. This would also help explain why the overall hardness is highest in the KG sample, as seen in figure 4.3, this is however not consistent across all the samples. The amount of carbide banding present would be expected to have an impact on the overall hardness, however, to which extent this effect is present is difficult to determine due to the presence of other microstructural constituents. The hardness in the carbide banded regions, seen in figure 4.5, indicates that the SL sample has a somewhat greater hardness than what is seen across the other samples. This indicates that the carbide bands present in this sample have a higher carbide density. Furthermore, it can be seen that the SK samples have a

greater standard deviation of hardness in the carbide bands. This is due to an inconsistent behavior of the carbide bands seen during microscopy. The hardness results would indicate that the carbide bands in the SL samples would be most detrimental due to the higher hardness of these bands.

Analysis of the types of carbides present in the material was done with the use of previous thermo-calc simulations, done by Lie Zhao at VDL Wewler, as well as XRD analysis. The thermo-calc simulations found that the predominate carbide type present was M3C, with a max fraction of 6.58%. Smaller fractions of M73C and MC were also found to be present with a max fraction of 2.61% and 1.94% respectively. The XRD analysis found similar results as a cementite phase fraction of 6% was detected and a FCC phase fraction of 1%. Due to overlap in the crystal structure, the M3C and M73C carbides would be expected to correspond with the cementite measured during XRD analysis. Furthermore, the MC carbides have a FCC crystal structure which would correspond with the 1% phase fraction of FCC measured during XRD. Overall, this would indicate that the max carbide fraction would be 7%, however, this is likely lower due to the presence of cementite.

Analysis of the carbide banding area as a function of depth can be seen in figure 4.6. This analysis indicates that carbide band formation in the SL sample starts more closely to the surface. The formation of carbide bands in samples SL and SC increases rapidly towards the center after which a plateau in the relationship can be seen. Carbide band formation in the SK and KG samples is more gradual and doesn't peak until the center of the sample. This analysis shows similar results to what was seen in the microscopy analysis.

The micro-segregation was analyzed using EPMA. The results of the EPMA can be seen in figure 4.7. This analysis indicated that for all the samples the micro-segregation spacing increases as a function of surface depth. This follows what was expected according to literature. The amount at which the spacing increases tend to differ across the samples. As for the SC sample, the micro-segregation spacing increases significantly towards the center whilst this is much less the case for the KG sample. Furthermore, the SL sample shows a much more significant increase from the surface to 25% from the surface compared to 25% from the surface to the center, whilst the opposite is the case for the SK sample. From these results, any relationship between the micro-segregation spacing and the carbide band formation cannot be found.

The micro-segregation peak concentration also increases towards the center, which was also expected from literature. The micro-segregation peak concentration was relatively consistent at both the surface and the center across all the samples. Large differences could be seen for the micro-segregation peak concentration at 25% from the surface. The SL sample has a much greater micro-segregation peak concentration whilst the SC sample has a much lower micro-segregation peak concentration at 25% from the surface. The difference in micro-segregation peak concentration at this depth helps explain why the formation of carbide bands occurs closer to the surface for the SL sample and further from the surface for the SC sample as seen in the microscopy and band area analysis. A clear relationship between the micro-segregation peak concentration and the carbide band formation can be seen. Further EPMA analysis would be necessary to confirm if the micro-segregation peak concentration is consistent in the region where carbide banding occurs. This would indicate the minimum micro-segregation degree for carbide banding to occur. This would be expected to be approximately what is seen for the SC sample at 25% from the surface, namely, at approximately 1.37% chemical concentration for chromium or 20% greater than the mean concentration. Further measurements would help to understand the relationship between carbide band concentration and micro-segregation.

Next to the micro-segregation, the macro-segregation was also investigated. Macro-segregation is not expected to have as significant of an impact on carbide band formation as micro-segregation. However, macro-segregation could lead to an increased amount of micro-segregation towards the center and hence impact the carbide band formation. Macro-segregation in terms of increased chemical concentration towards the center is quite common. However, this is quite dependent on the concentration of alloying elements present in the steel and therefore highly dependent on the steel grade. A small amount of macro-segregation was found for the manganese in the EPMA results for the KG and SL samples. The more extensive EDS research did not indicate any clear macro-segregation behavior for

manganese in these samples, however. Furthermore, no macro-segregation could be seen amongst the other alloying elements in any of the samples. This likely indicated that macro-segregation is uncommon for 51CrV4 steel as this behavior is consistent across steel from different manufacturers.

The EDS analysis of the carbide regions helps understand the chemical concentration of these regions which helps indicate the predominant type of carbide present in these regions. Of the potential carbide-forming elements, chromium is the only one that is consistently present amongst the banded regions for all of the samples. The vanadium concentration is greater in these regions compared to the overall concentration, which might indicate the presence of vanadium carbide. However, this is not consistent across all banded regions, indicating it is not present in all of the carbide banded regions. It has also been found that the inconsistency in the presence of manganese in these regions can be linked to the presence of sulfur. This indicates that the formation of manganese sulfides tends to occur in areas where sulfur and manganese are present. These manganese sulfides can often be clearly seen in the microscope and SEM images as a darker microstructure found with the carbide bands as seen in the appendix in figure A.15. Overall, this would indicate that chromium carbides would be expected to be the primary carbide former in these regions. The EDS analysis of the carbide bands also indicated that the relationship between carbide band chemical concentration and surface depth tends to differ somewhat across the steel from different manufacturers. The chromium concentration increases significantly for the carbide banded regions towards the center of the KG sample. This is also the case for the SK sample to a lesser extent. The chemical concentration of chromium in carbide bands in the SC and SL samples tended to remain consistent as a function of the surface depth. These results help explain the difference in built up of the carbide band area for the different samples. The increase in the chemical concentration of chromium towards the center of the KG and SK samples helps explain why the carbide band area increases more gradually towards the center of these samples. Whilst, the SC and SL samples see the largest increase in carbide area at the initiation depth of carbide banding with a subsequent plateau in concentration.

6

Conclusions and Recommendations

6.1. Conclusions

The primary goal of the research was to understand the relation between the surface depth and band formation in 51CrV4 steel and how banding differs for 51CrV4 steel from different manufacturers. In order to achieve this, sub-research goals were set up. These goals were to correlate the impact of surface depth to band formation, determine the depth at which band formation starts, investigate the underlying micro-segregation and the impact it has on band formation and identify the predominate banding microstructure found in 51CrV4 steel.

The impact of surface depth on band formation was researched using optical microscope images and SEM images. It was found that the band formation tends to start in a similar surface depth range for the different steel samples investigated. Band formation, however, was found to start nearest to the surface for the SL samples with an average band start depth of 16.55% from the surface. Band formation started furthest from the surface for the SC samples at 25.18% on average. The SEM analysis showed similar results as the band area analysis of the SL sample; Indicating that the band formation occurred at an earlier stage for the SL sample followed by a rapid increase and subsequent plateau in band area fraction. The SC sample also showed a rapid increase in band area after the band start depth followed by a plateau in area fraction. The buildup of the band fraction in the KG and SK samples was found to be more gradual and does not peak until the center. This would indicate that the formation of carbide bands would be expected to be most detrimental in the SL sample and least detrimental in the SC sample. This is due to carbide bands that form more closely to the surface, where the external stresses are the highest, having a more adverse impact on the mechanical properties of the steel.

It was found that the depth at which the carbide bands tended to form could be most closely related to the micro-segregation peak concentration. It can be seen that the SC sample has the highest peak concentration of chromium at 25% from the surface whilst the SL sample has the lowest peak concentration, which corresponds well with what was found in the microscope and SEM analysis. It could be seen that the micro-segregation spacing increases as a function of surface depth. However, the micro-segregation spacing tended to differ across the sample making it difficult to correlate it to the band formation.

The hardness results indicated that the hardness of the samples tended to decrease as a function of surface depth. This was primarily due to increased ferrite being present towards the center of the samples compared to the tempered martensite near the surface. These microstructures are more predominantly present in these regions due to the decreased cooling rates experienced towards the center. The combination of increased concentration of ferrite and carbides towards the center also leads to a

larger standard deviation in hardness measurements towards the center. It was found that the hardness in the carbide banded regions was significantly higher than in the surrounding regions. Furthermore, it was seen that the hardness in the carbide band regions of the SL samples was particularly high. This is most likely due to an increased concentration of carbides present in these regions. This would likely result in an adverse impact on the mechanical properties in the SL sample as the increased hardness in these regions could lead to increased crack formation and propagation.

The EDS results of the carbide banded regions indicate that the primary carbide former in this region is chromium. This is due to the chromium concentration in these regions remaining consistently high throughout the carbide banded regions whilst vanadium and manganese concentrations have a large variation across the different bands in the banded regions. Furthermore, the presence of large concentrations of manganese in the carbide banded region has been found to correspond with high concentrations of sulfur. This would indicate that manganese sulfides are present in these areas. These manganese sulfides can often be clearly seen in SEM images of the bands with increased sulfur and manganese concentrations. The primary carbide type expected to be present is the M3C carbide with a smaller fraction of M73C and MC. The maximum carbide fraction according to XRD analysis is 7%, however, this is likely lower due to the presence of cementite.

6.2. Recommendations

In order to further the results of this thesis and the influence of carbide banding in 51CrV4 Steels, the following is recommended for further research:

- Further analysis using EPMA, where the full depth of samples are analyzed as well as multiple measurements per sample, is recommended. This would help in correlating the micro-segregation behavior to the band formation. This would also help in determining if there is a minimum segregation degree required for carbide banding to occur.
- Further research into the types of carbides present and their concentration in the material would be recommended. This could be done in a number of ways, however, EBSD analysis would likely be the most effective in this.
- This research focused on the transverse phase, thereby relating the carbide bands (orientated along the rolling direction) which the surface depth with respect to the normal direction. Further research into how the carbide bands develop as a function of the surface depth along the transverse direction would be recommended.
- This research focused on the carbide banding behavior in the thickest region of the trailing arm. It would be recommended to compare this behavior to other sections of the trailing arm. These regions would therefore undergo further elongation due to hot-rolling, which could have a significant impact on the carbide banding behavior and the micro-segregation.

A

Appendix

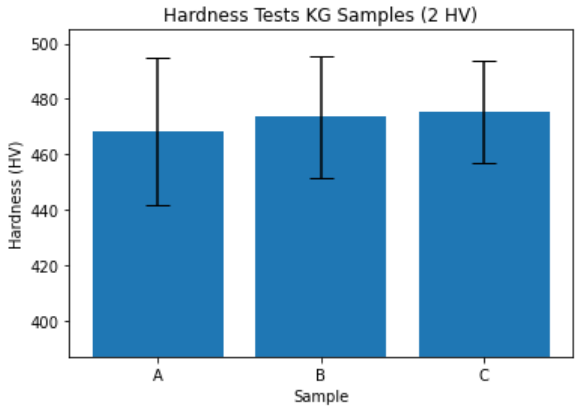

(a) KG

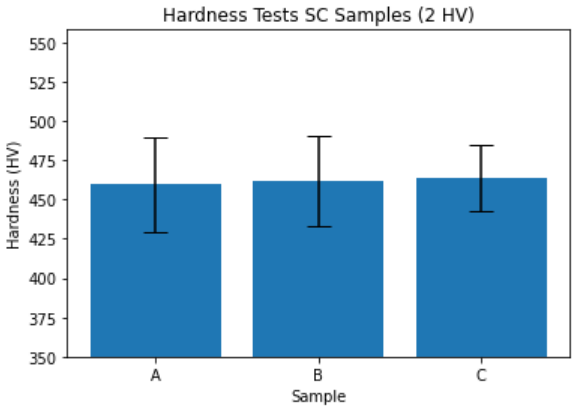

(b) SC

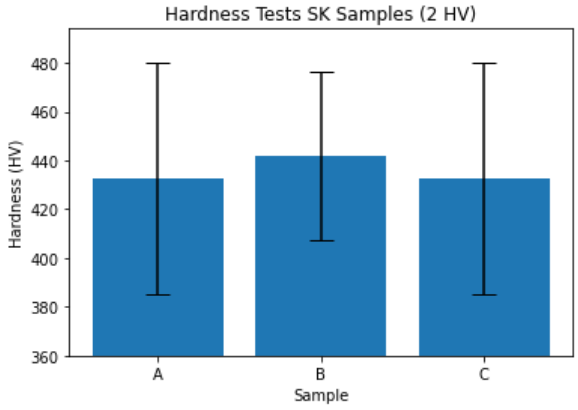

(c) SK

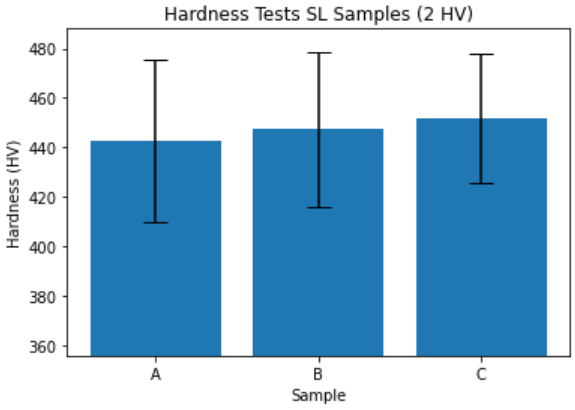

(d) SL

Figure A.1: Box chart of the hardness test for each steel manufacturer separated based on the sample used. The figure indicates the average hardness for each sample as well as the expected range based on the data.

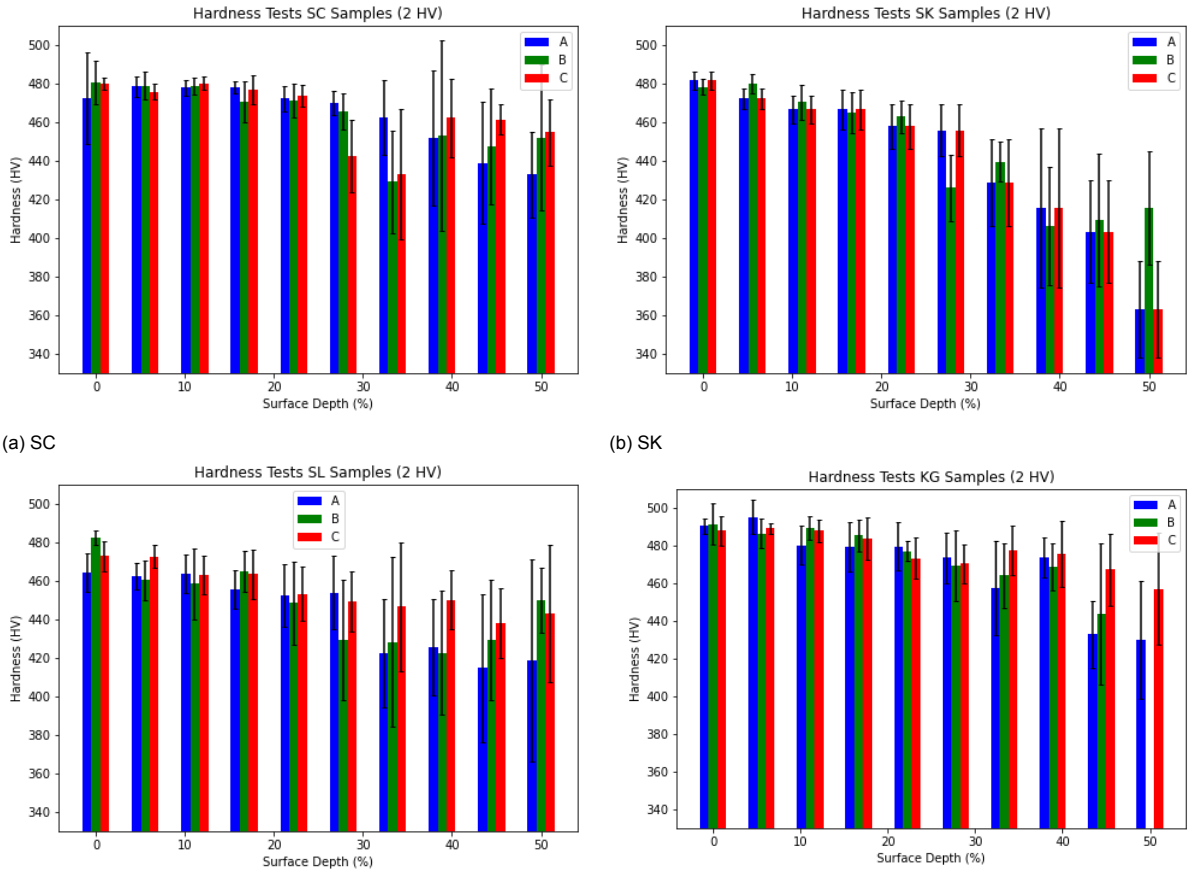

(a) SC

(b) SK

(c) SL

(d) KG

Figure A.2: Hardness measurements of each samples as a function of depth. Measurements range from the surface (0%) to the center (50%).

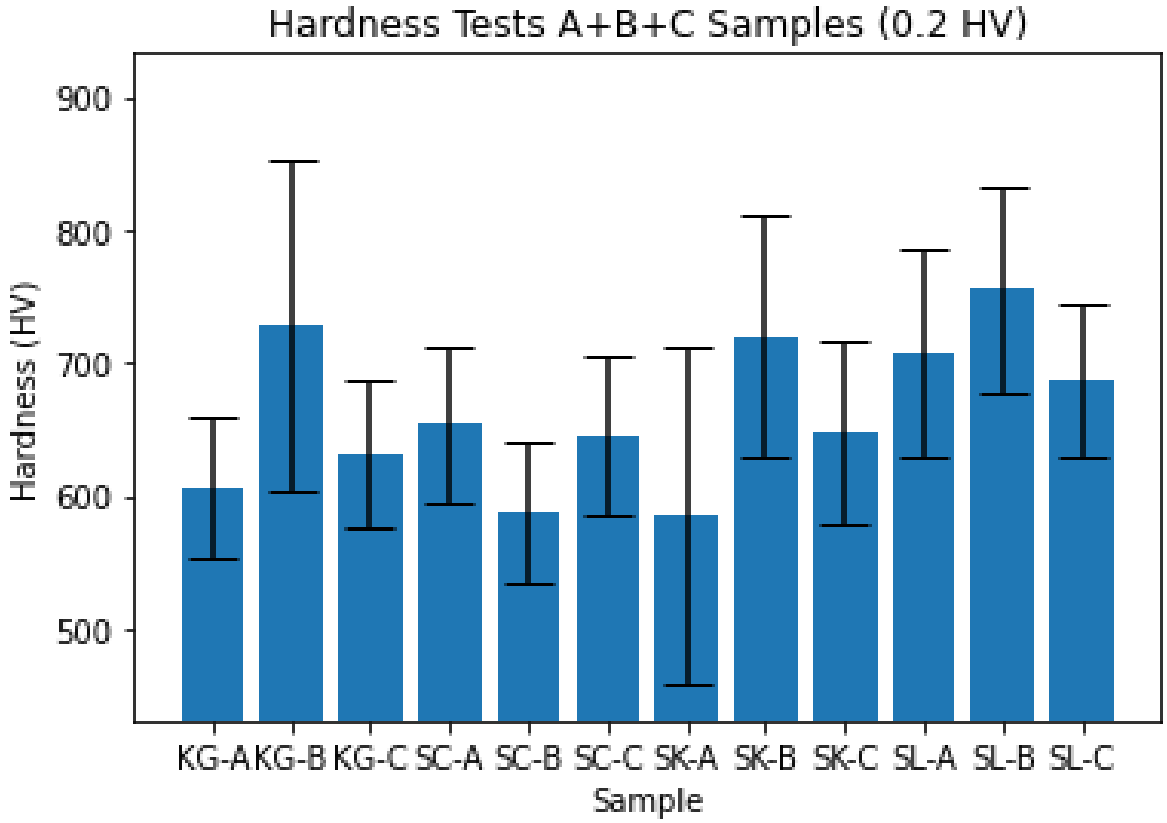

Figure A.3: Average hardness in the carbide banding regions for each individual samples measured.

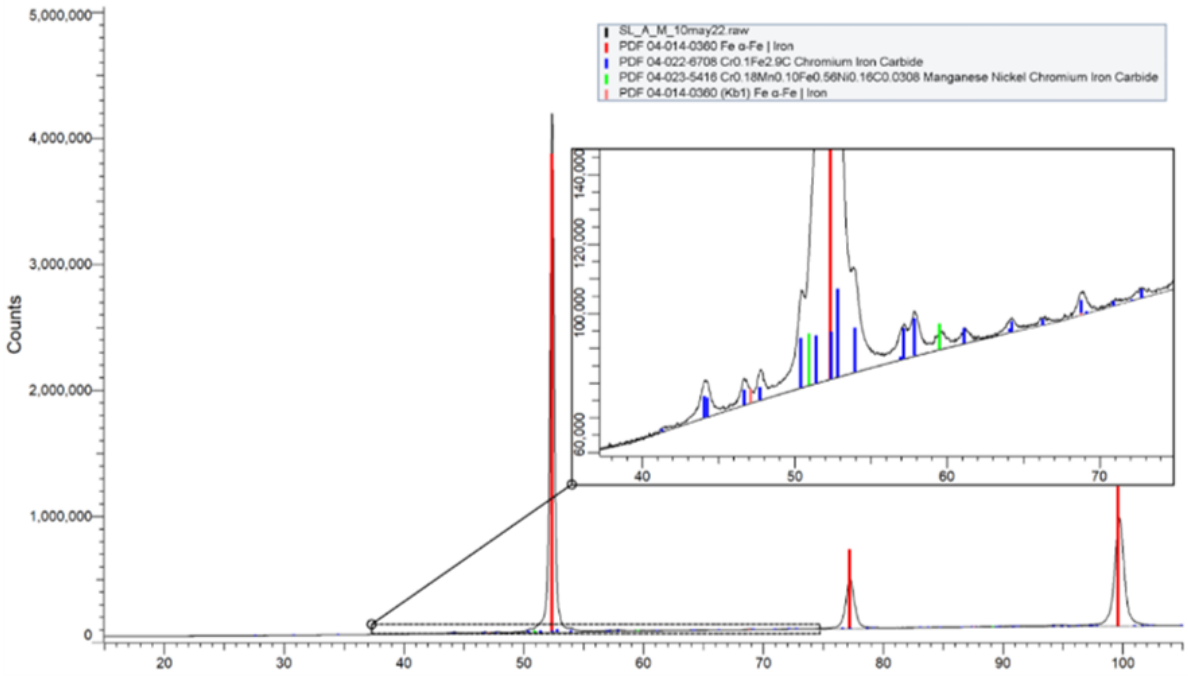

Figure A.4: XRD analysis showing the measured peaks from the analysis as well as the predicted location of the corresponding phases. These results where used to determine the phase fraction in the 51CrV4 samples.

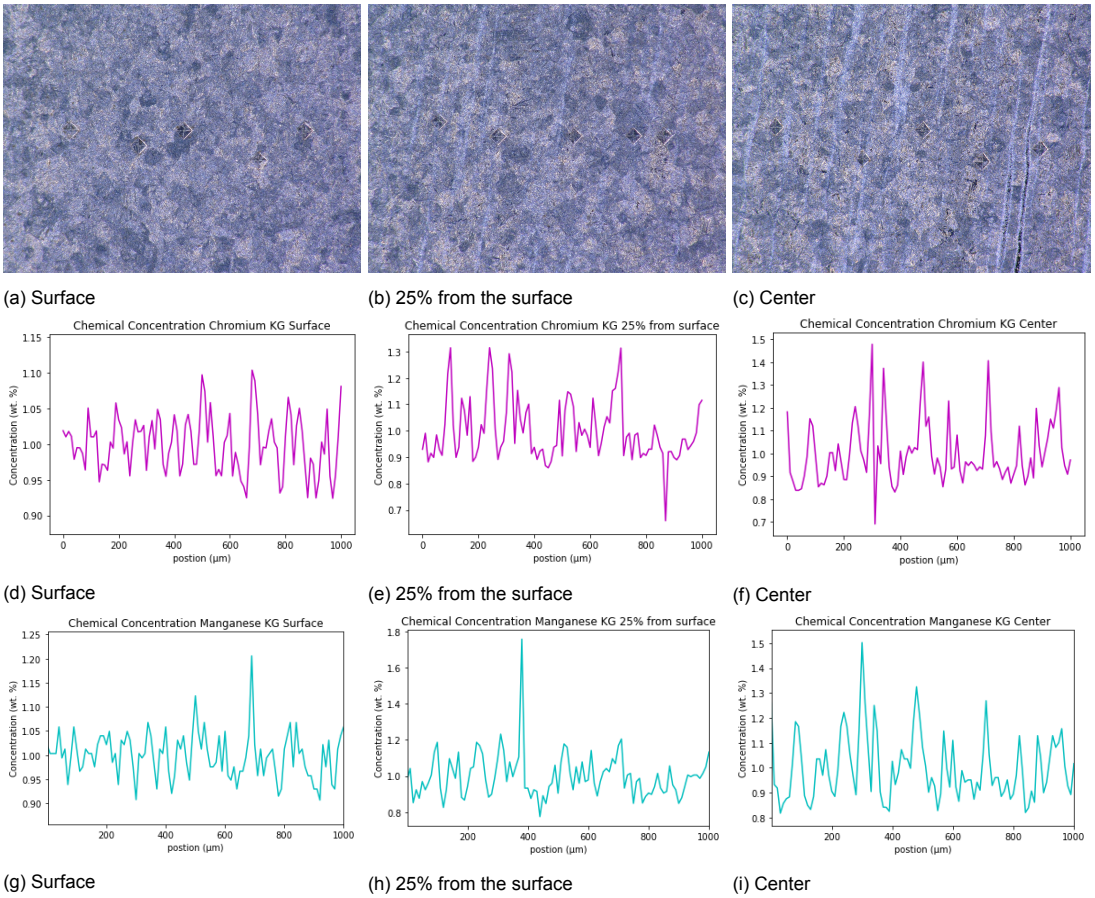

(a) Surface (b) 25% from the surface (c) Center

(d) Surface (e) 25% from the surface (f) Center

(g) Surface (h) 25% from the surface (i) Center

Figure A.5: EPMA results of chromium in the KG sample measured at A.5d) The surface, A.5e) 25% from the surface and A.5f) The center of the sample. EPMA results of manganese in the KG sample measured at A.5g) The surface, A.5h) 25% from the surface and A.5i) The center of the sample. In figure A.5a, A.5b and A.5c the corresponding microscope images can be seen.

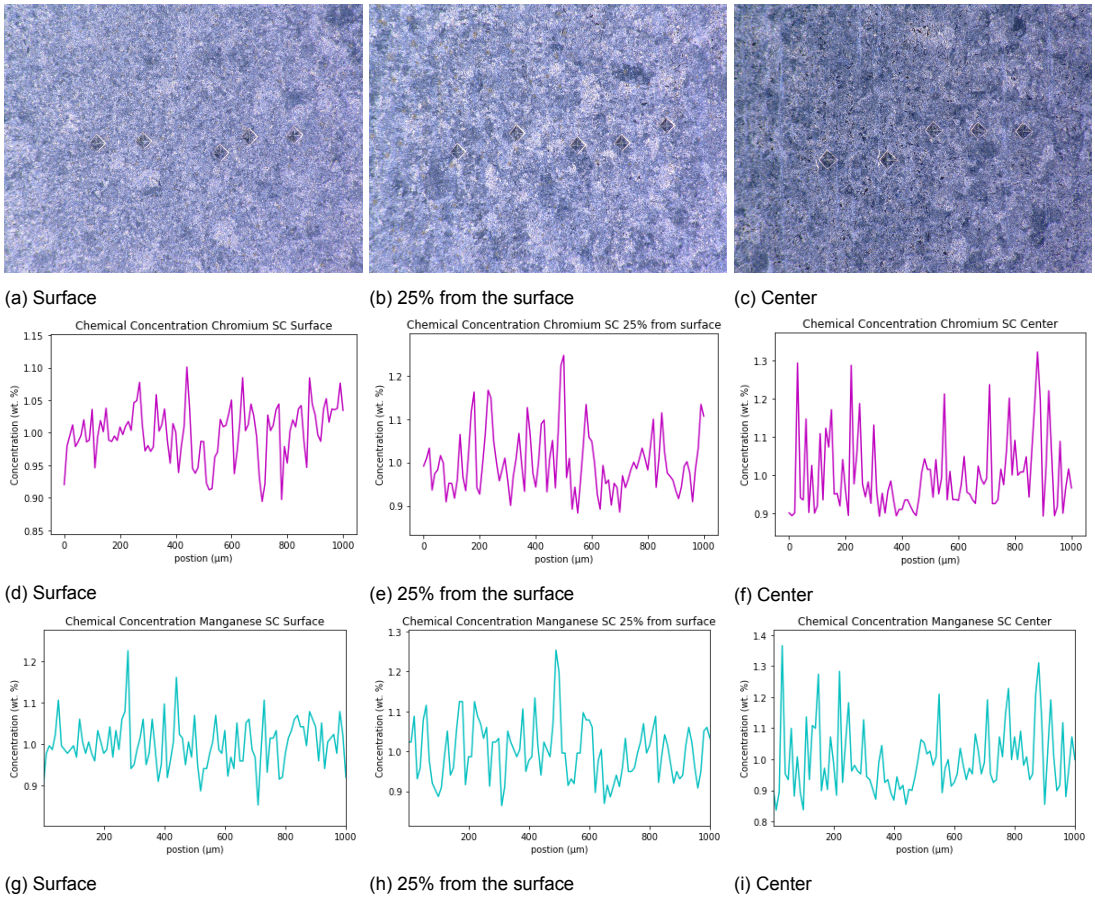

Figure A.6: EPMA results of chromium in the SC sample measured at A.6d) The surface, A.6e) 25% from the surface and A.6f) The center of the sample. EPMA results of manganese in the SC sample measured at A.6g) The surface, A.6h) 25% from the surface and A.6i) The center of the sample. In figure A.6a, A.6b and A.6c the corresponding microscope images can be seen

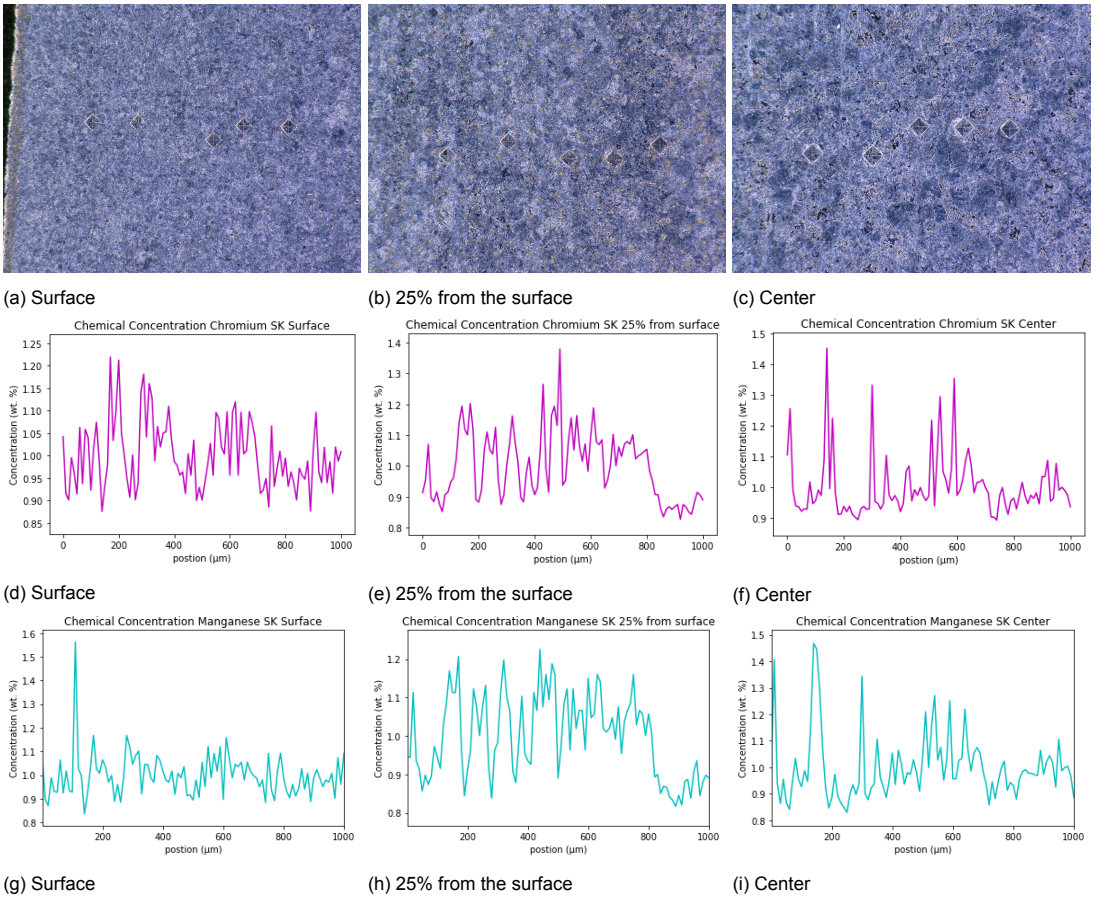

Figure A.7: EPMA results of chromium in the SK sample measured at A.7d) The surface, A.7e) 25% from the surface and A.7f) The center of the sample. EPMA results of manganese in the SK sample measured at A.7g) The surface, A.7h) 25% from the surface and A.7i) The center of the sample. In figure A.7a, A.7b and A.7c the corresponding microscope images can be seen.

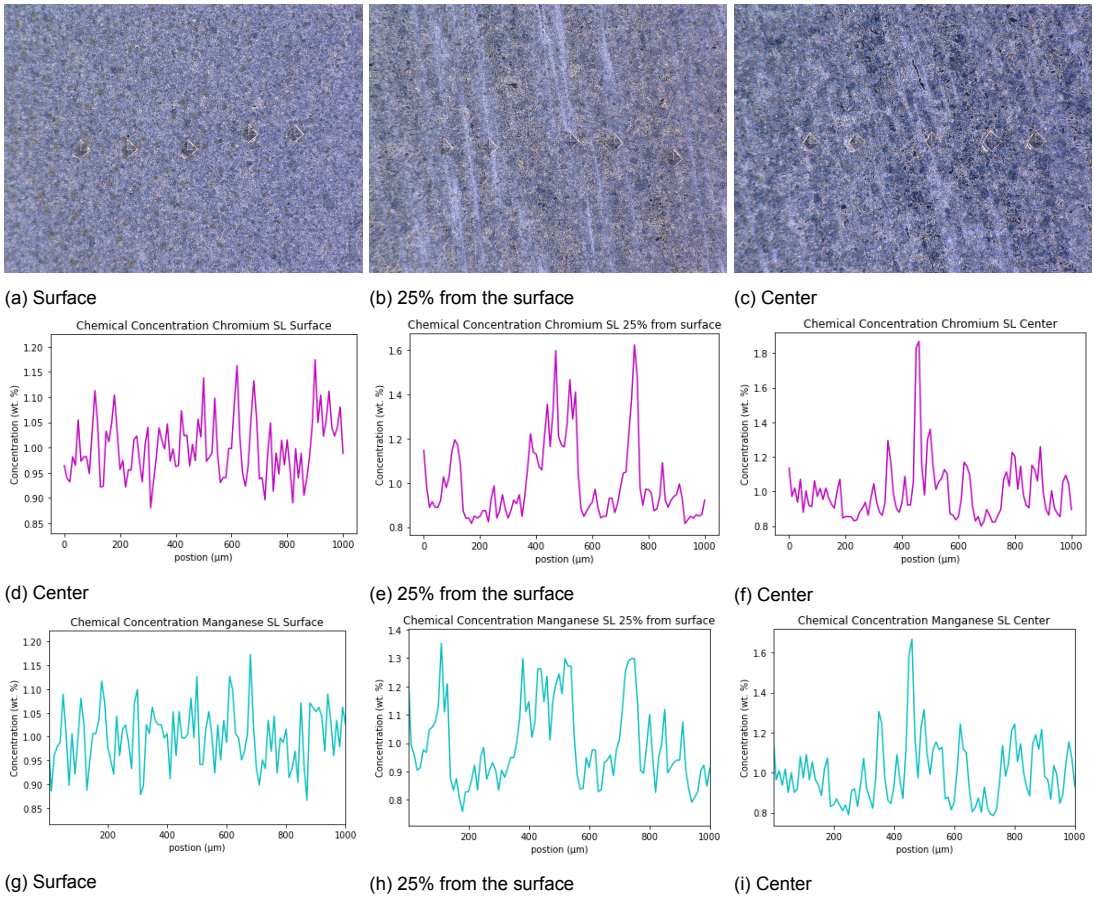

Figure A.8: EPMA results of chromium in the SL sample measured at A.8d) The surface, A.8e) 25% from the surface and A.8f) The center of the sample. EPMA results of manganese in the SL sample measured at A.8g) The surface, A.8h) 25% from the surface and A.8i) The center of the sample. In figure A.8a, A.8b and A.8c the corresponding microscope images can be seen.

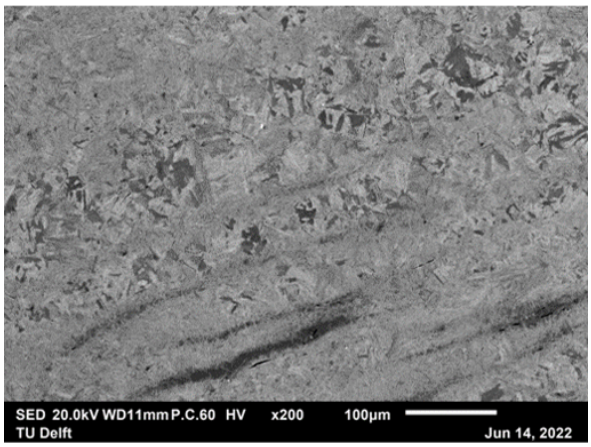

(a) SEM image

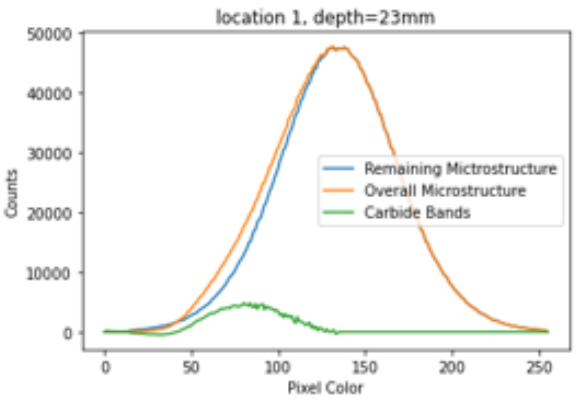

(b) Grey scale analysis of the SEM image

Figure A.9: Overview of how the band area analysis was conducted. In figure A.9a a SEM image of the samples can be seen. In figure A.9b the grey scale analysis of the SEM image can be seen with the Carbide banded area and the remaining microstructure being separated from each other. From the difference the carbide band area can be determined.

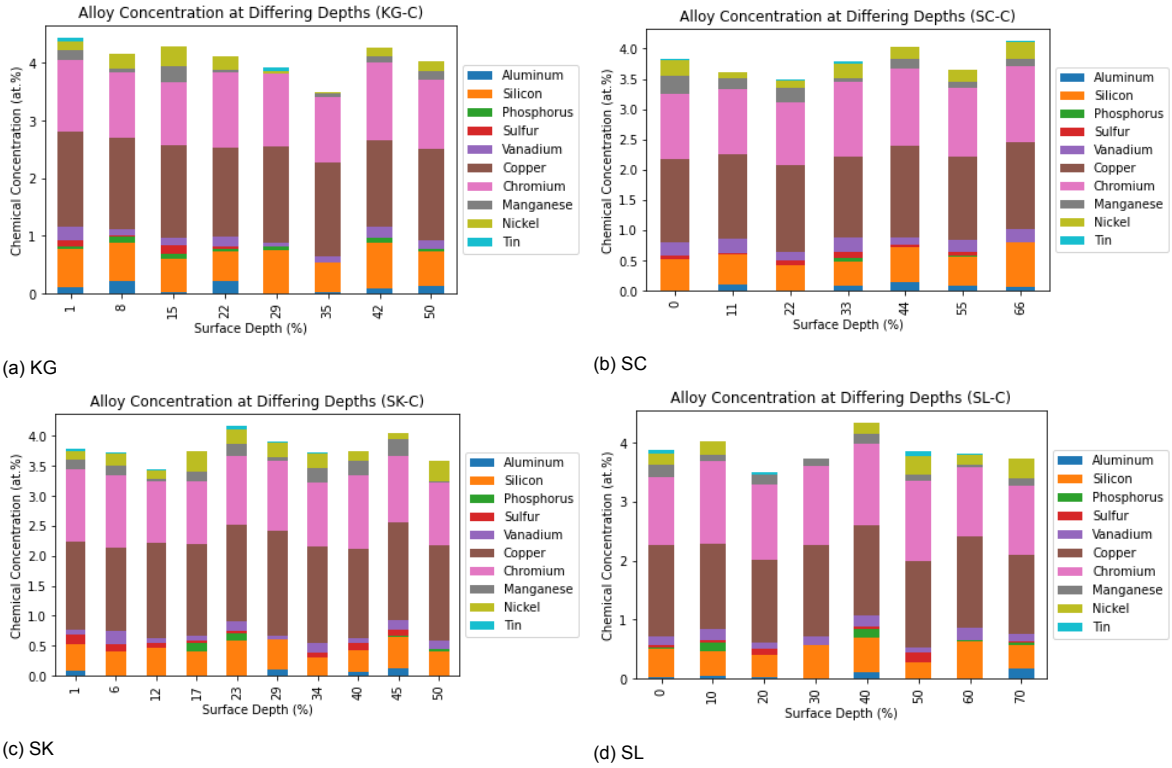

(a) KG

(b) SC

(c) SK

(d) SL

Figure A.10: Overview of the micro-segregation of all the elements present in the microstructure for the samples of all the manufacturers based on the EDS results. The figure that corresponds with each manufacturer is indicated in the sub-figure.

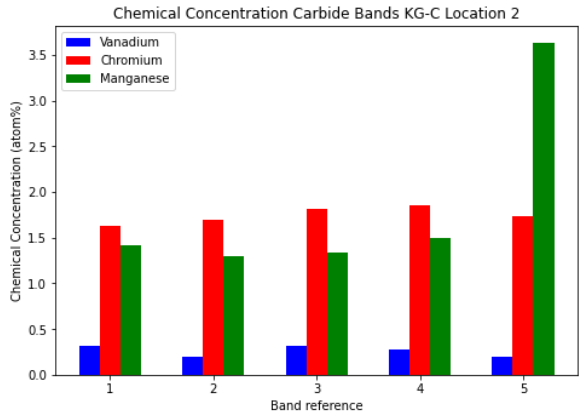

(a) KG Carbide Band 1

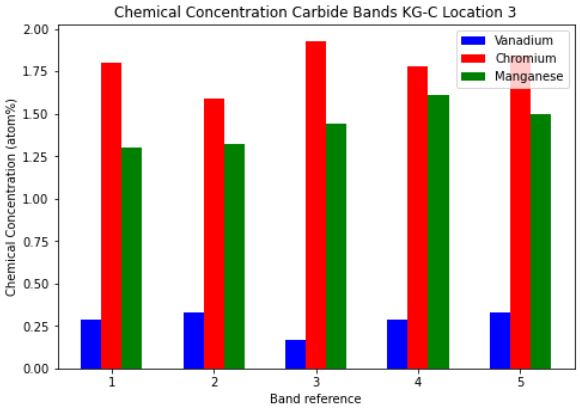

(b) KG Carbide Band 2

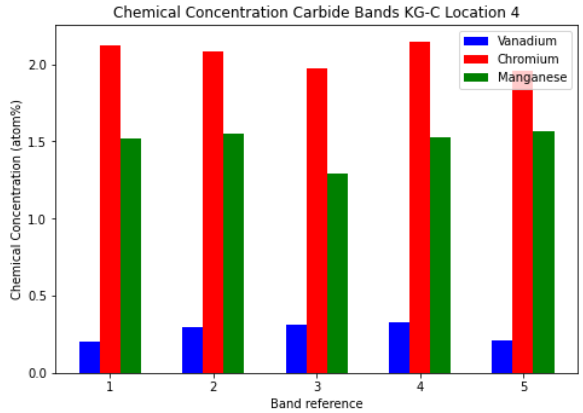

(c) KG Carbide Band 3

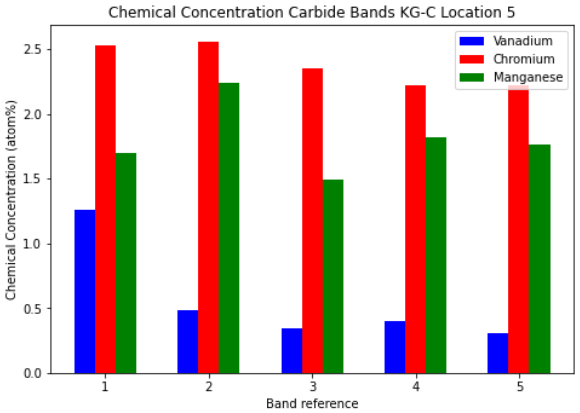

(d) KG Carbide Band 4

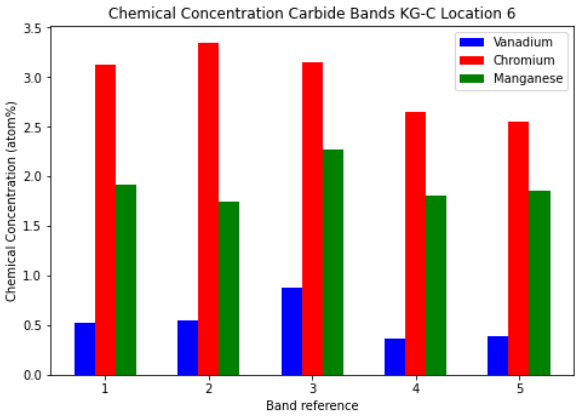

(e) KG Carbide Band 5

Figure A.11: Overview of the different EDS measurements made in the KG sample. Band 1 is closest to the surface whilst band 5 is closest to the center.

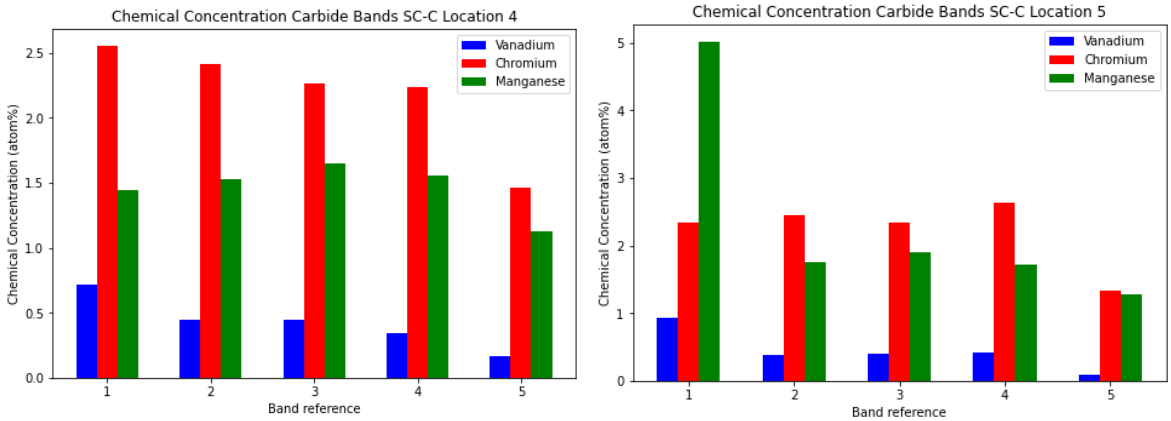

(a) SC Carbide Band 1

(b) SC Carbide Band 2

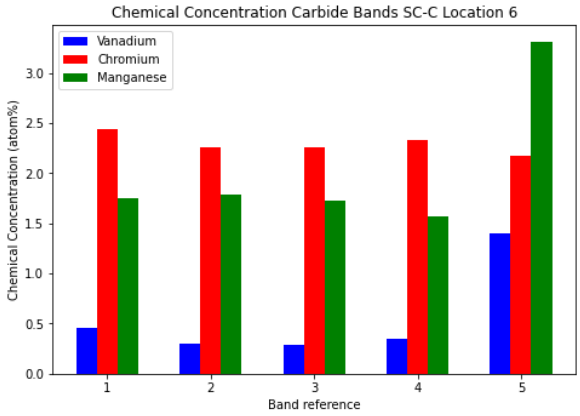

(c) SC Carbide Band 3

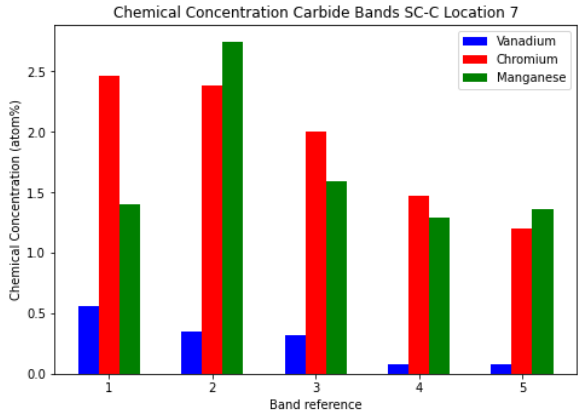

(d) SC Carbide Band 4

Figure A.12: Overview of the different EDS measurements made in the SC sample. Band 1 is closest to the surface whilst band 5 is closest to the center.

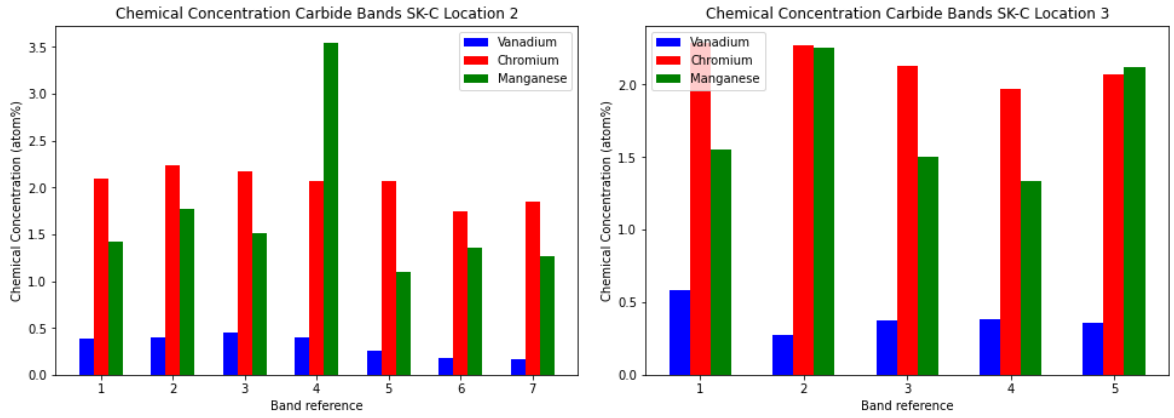

(a) SK Carbide Band 1

(b) SK Carbide Band 2

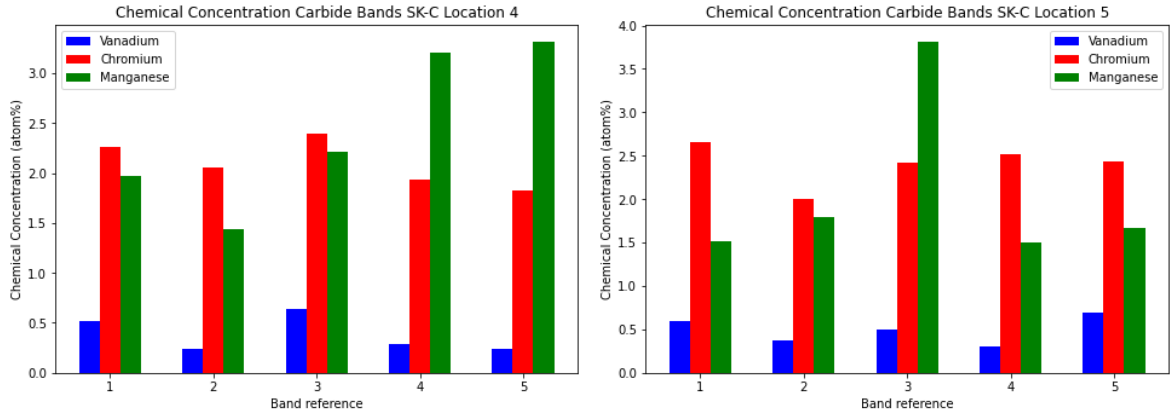

(c) SK Carbide Band 3

(d) SK Carbide Band 4

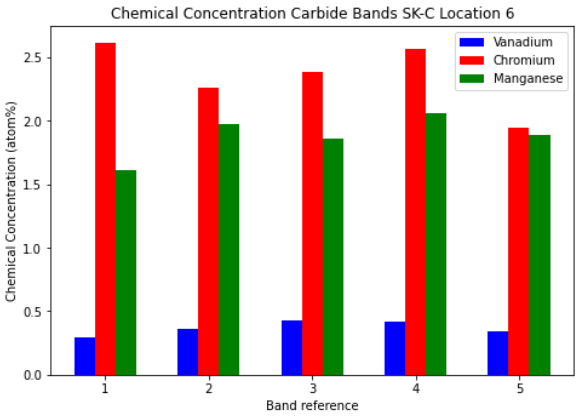

(e) SK Carbide Band 5

Figure A.13: Overview of the different EDS measurements made in the SK sample. Band 1 is closest to the surface whilst band 5 is closest to the center.

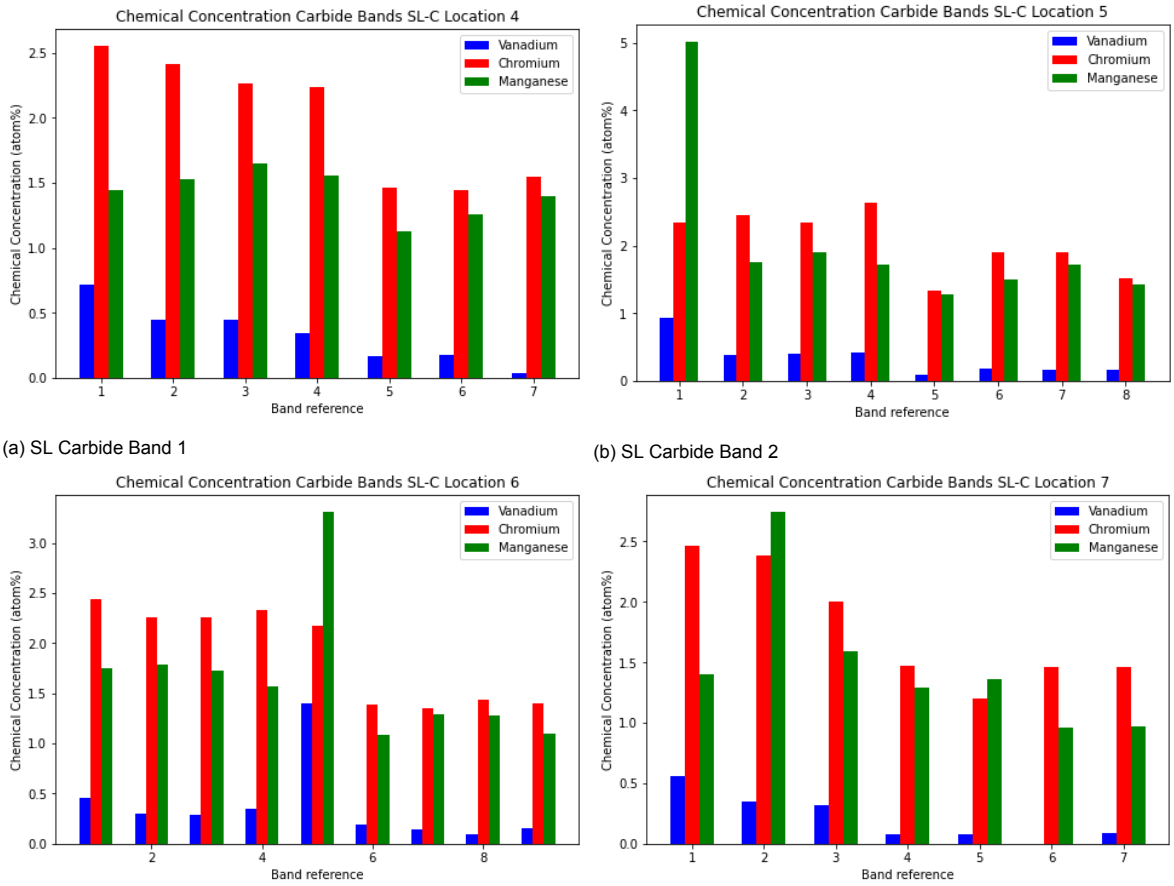

(a) SL Carbide Band 1

(b) SL Carbide Band 2

(c) SL Carbide Band 3

(d) SL Carbide Band 4

Figure A.14: Overview of the different EDS measurements made in the SL sample. Band 1 is closest to the surface whilst band 5 is closest to the center.

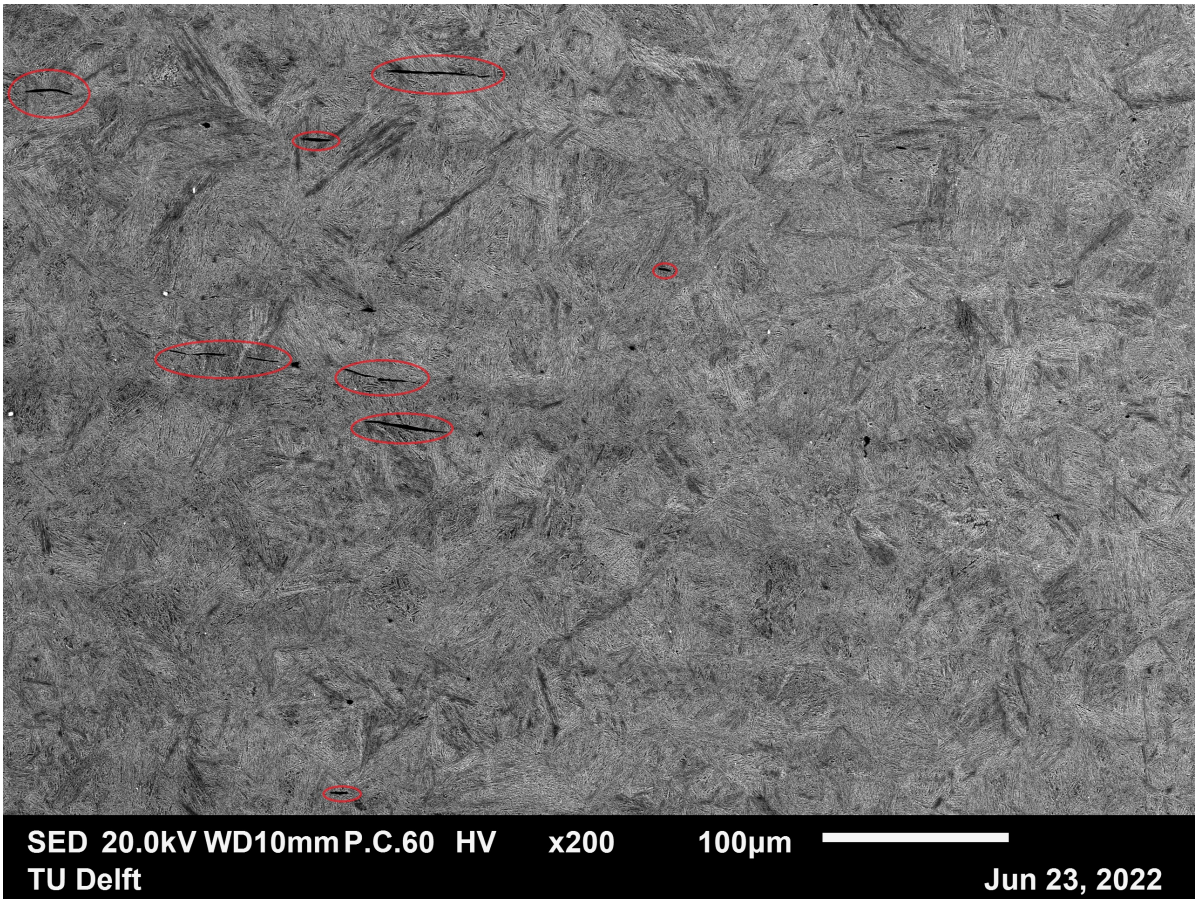

Figure A.15: Overview of Manganese Sulphide inclusions found throughout the sample. The MnS inclusions can be seen as a dark long and thin microstructure. In this figure the MnS inclusions are indicated with red circles.

Bibliography

[1] Masoud Al Gahtani. “Formation of micro-structural banding in hot-rolled medium-carbon steel”. In: *University of Wollongong Thesis Collections* (2015).

[2] Joel Beckham and Daniel Beggs. *51CrV4 Quenched and Tempered Steels Overview*. 2019.

[3] H D Brody and M C Flemmings. *Solute redistribution in dendritic solidification*. 1966.

[4] A.W. Cramb. “Casting of Near Net Shape Products”. In: *TMS* (1988), pp. 673–682.

[5] H. Farahani, W. Xu, and S. van der Zwaag. “A Novel Approach for Controlling the Band Formation in Medium Mn Steels”. In: *Metallurgical and Materials Transactions A: Physical Metallurgy and Materials Science* 49.6 (2018), pp. 1998–2010. ISSN: 10735623. DOI: 10.1007/s11661-018-4565-8.

[6] U Feurer and R Wunderlin. “Fachbericht der DGM-FB-38/667”. In: *DGM-Informationsgesellschaft-Verlag* (1977), p. 38.

[7] M.C. Flemings and G.E. Nereo. “Macrosegregation: Part I”. In: *Trans. Metall. Soc. AIME* 239 (1967), pp. 1449–146.

[8] Eric A Jägle. “Modelling of Microstructural Banding during Transformations in Steel”. In: *University of Cambridge Department of Materials Science & Metallurgy* August (2007), p. 63.

[9] J. S. Kirkaldy, J. von Destinon-Forstmann, and R. J. Brigham. “Simulation of Banding in Steels”. In: *Canadian Meallurgical Quarterly* (1963), pp. 59–81.

[10] Theo Kop. *A dilatometric study of the austenite/ferrite interface mobility*. 2000. URL: https://repository.tudelft.nl/islandora/object/uuid:2660ecb3-c89e-4fd4-a12a-3e5687f2fee6?collection=research.

[11] George Krauss. “Solidification, Segregation, and Banding in Carbon and Alloy Steels”. In: *Metallurgical and Materials Transactions B: Process Metallurgy and Materials Processing Science* 34.6 (2003), pp. 781–792. ISSN: 10735615. DOI: 10.1007/s11663-003-0084-z.

[12] E Leonard. *Microscopy of Carbon Steels*. 1999, p. 342. URL: www.knovel.com.

[13] Z. Morita and Toshihiko Emi. “An introduction to iron and steel processing”. In: *The Foundation* (1997).

[14] S. E. Offerman et al. “Ferrite/pearlite band formation in hot rolled medium carbon steel”. In: *Materials Science and Technology* 18.3 (2002), pp. 297–303. ISSN: 02670836. DOI: 10.1179/026708301225000752.

[15] Robert Pierer and Christian Bernhard. “On the influence of carbon on secondary dendrite arm spacing in steel”. In: *Journal of Materials Science* 43.21 (2008), pp. 6938–6943. ISSN: 00222461. DOI: 10.1007/s10853-008-2985-3.

[16] Hubert Preßlinger et al. “Assessment of the primary structure of slabs and the influence on hot- And cold-rolled strip structure”. In: *Steel Research International* 77.2 (2006), pp. 107–115. ISSN: 16113683. DOI: 10.1002/srin.200606362.

[17] Hubert Preßlinger et al. “Methods for assessment of slab centre segregation as a tool to control slab continuous casting with soft reduction”. In: *ISIJ International* 46.12 (2006), pp. 1845–1851. ISSN: 09151559. DOI: 10.2355/isijinternational.46.1845.

[18] G. R. Purdy and J. S. Kirkaldy. “Homogenization by diffusion”. In: *Metallurgical Transactions* 2.2 (1971), pp. 371–378. ISSN: 03602133. DOI: 10.1007/BF02663324.

[19] Orhan Sadettin, Öztürk Fahrettin, and Gattmah Jabbar. “Analysis of Cold Rolling Process With Different Parameters Using Finite Element Method”. In: *1st International Conference on Advances in Mechanical and Mechatronics Engineering (ICAMMEN 2018), 8-9 November 2018* January 2019 (2018), pp. 354–360. URL: http://aybu.edu.tr/icammen2018/.

[20] E Scheil. “Bemerkungen zur schichtkristallbildung”. In: *Zeitschrift für Metallkunde* 34.3 (1942), pp. 70–72.

[21] S. Steinbach and L. Ratke. “Effects of controlled convections on dendritic microstructure and segregation during microgravity-solidification”. In: *European Space Agency, (Special Publication) ESA SP* 647 SP (2007), pp. 373–378. ISSN: 03796566.

[22] Akira Suzuki et al. *On Secondary Dendrite Arm Spacing in Commercial Carbon Steels with Different Carbon Content*. 1968. DOI: 10.2320/jinstmet1952.32.12{_}1301.

[23] S. W. Thompson and P. R. Howell. “Factors influencing ferrite/pearlite banding and origin of large pearlite nodules in a hypoeutectoid plate steel”. In: *Materials Science and Technology (United Kingdom)* 8.9 (1992), pp. 777–784. ISSN: 17432847. DOI: 10.1179/mst.1992.8.9.777.

[24] Y. Tomita. “Effect of modified austemper on tensile properties of 0·52%C steel”. In: *Materials Science and Technology (United Kingdom)* 11.10 (1995), pp. 994–997. ISSN: 17432847. DOI: 10.1179/mst.1995.11.10.994.

[25] George E. Totten. *Steel Heat Treatment*. Ed. by CRC Press. Second Edi. st, 2006.

[26] E.T. Turkdogan and R.A. Grange. “Microsegregation in Steel”. In: *Journal of the Iron and Steel Institute* (1970), pp. 482–494.

[27] John D. Verhoeven. “Review of microsegregation induced banding phenomena in steels”. In: *Journal of Materials Engineering and Performance* 9.3 (2000), pp. 286–296. ISSN: 10599495. DOI: 10.1361/105994900770345935.

[28] John D. Verhoeven. *Steel Metallurgy for the Non-Metallurgist*. 2007, pp. 1–4. DOI: 10.31399/asm.tb.smnm.t52140001.

[29] Hong Yi Wu et al. “Effect of Cooling Rate on Carbide Banding in High-Chromium Bearing Steel After Spheroidization”. In: *Metallurgical and Materials Transactions A: Physical Metallurgy and Materials Science* 51.9 (2020), pp. 4471–4482. ISSN: 10735623. DOI: 10.1007/s11661-020-05870-6. URL: https://doi.org/10.1007/s11661-020-05870-6.